



**HAL**  
open science

# Quasi-symmetrical contact algorithm and recurrent boundary conditions: application to 3d metal forging simulations

Sorin Popa

► **To cite this version:**

Sorin Popa. Quasi-symmetrical contact algorithm and recurrent boundary conditions: application to 3d metal forging simulations. Engineering Sciences [physics]. École Nationale Supérieure des Mines de Paris, 2005. English. NNT : 2005ENMP1422 . pastel-00002047

**HAL Id: pastel-00002047**

**<https://pastel.hal.science/pastel-00002047>**

Submitted on 11 Jun 2007

**HAL** is a multi-disciplinary open access archive for the deposit and dissemination of scientific research documents, whether they are published or not. The documents may come from teaching and research institutions in France or abroad, or from public or private research centers.

L'archive ouverte pluridisciplinaire **HAL**, est destinée au dépôt et à la diffusion de documents scientifiques de niveau recherche, publiés ou non, émanant des établissements d'enseignement et de recherche français ou étrangers, des laboratoires publics ou privés.





## **Remerciements**

Cette thèse a été effectuée au Centre de Mise en Forme des Matériaux (CEMEF) de l'École Nationale Supérieure des Mines de Paris. Je voudrais remercier à la direction de l'École des Mines et particulièrement à Monsieur Jean Loup Chenot, qui a dirigé mon stage initial au sein de CEMEF après lequel il m'a proposé le contrat de thèse, malgré mon manque d'expérience dans les domaines de la mise en forme et les mathématiques appliquées.

Cette thèse n'aurait vu le jour sans la confiance, la patience et la générosité de mon directeur de recherche, Monsieur Lionel Fourment, que je veux vivement remercier. De plus, les conseils qu'il m'a divulgué tout au long de la rédaction, ont toujours été clairs et succincts, me facilitant grandement la tâche et me permettant d'aboutir à la production de cette thèse.

Je remercie les rapporteurs de cette thèse, M. Laurent Baillet et M. José M.A. César de Sá pour la rapidité avec laquelle ils ont lu mon manuscrit et l'intérêt qu'ils ont porté à mon travail. Merci également aux autres membres du jury qui ont accepté de juger ce travail, M. Serge Cescotto et M. Richard Ducloux.

Un grand merci pour tout l'équipe de CEMEF pour m'avoir fourni d'excellentes conditions logistiques et financières et tout particulièrement à Monsieur Patrick Coels qui m'a soutenu dans ma démarche personnelle de « regroupement sentimental ».

Mes plus chaleureux remerciements s'adressent à Josué Barbosa, Ramzy Bousetta, Cyril Gruau, Olga Karasseva, Mihaela Teodorescu et tout les autres collègues pour leur soutien moral qu'ils m'ont fourni tout au long de la réalisation de ces travaux.



## INTRODUCTION, RESUME ET CONCLUSION EN FRANÇAIS

Cette thèse s'appuie sur deux articles en anglais publiés dans des revues internationales, aussi en proposons-nous une brève introduction.

Cette thèse faisait partie du projet national français Simulforge, qui réunissait plusieurs laboratoires de recherche et partenaires industriels de la forge, ainsi que le Centre technique des industries de la mécanique (CETIM) et Transvalor, l'éditeur du logiciel Forge3®.

Dans la première partie, la thèse traite de la réduction de temps de calcul pour la simulation du forgeage des engrenages hélicoïdaux. Sur la figure 1, on observe que les engrenages hélicoïdaux obéissent à un modèle de répétition. Il est donc possible de simuler le forgeage d'une seule dent. Le chapitre 2 décrit brièvement l'approche numérique du problème thermomécanique du forgeage. Dans le chapitre 3, on s'occupe plus en détails des conditions de symétries nécessaires pour effectuer la simulation du forgeage sur le domaine réduit à une seule dent. Ces conditions de symétries cycliques consistent à imposer que la matière qui sort d'une face de symétrie entre dans l'autre face. Cette condition se traduit par l'identité entre le champ de vitesse (chapitre 3.2) et de températures (chapitre 3.3) sur les deux surfaces de symétrie. Cette condition est très similaire à celle de contact collant entre les corps déformables, si on fait abstraction de la matrice de rotation introduite en sus. Donc, pour imposer cette condition de symétrie, un algorithme de type maître-esclave est nécessaire, semblable à celui utilisé pour traiter le contact entre les corps déformables. Dans le chapitre 3.2 on explique comment on obtient les différentes variables par l'algorithme de contact standard de Forge3® multi-corps, et comment on applique ensuite la condition de symétrie cyclique. Le chapitre 3.4 décrit comment gérer les nœuds qui se trouvent sur l'axe de symétries, nœuds qui peuvent seulement se déplacer sur l'axe. On bloque donc leurs degrés de liberté perpendiculaires à cet axe.

Un problème particulier se pose quand on doit simuler le forgeage avec des outils déformables. A cause de l'approche Lagrangienne utilisée, et éventuellement aussi à cause de la géométrie initiale, la matière d'une dent de la pièce ne s'écoule pas forcément dans une seule dent de l'outil. On explique, dans le chapitre 3.5, que multiplier la zone discrétisée de l'outil ne résout pas le problème. On est donc obligé d'écrire des conditions

aux limites particulières entre la pièce et l'outil. Ces conditions sont expliquées dans le chapitre 3.6. Elles consistent à écrire le contact entre les parties « libres » de la pièce de l'outil, en utilisant des outils virtuels qui peuvent être multipliés autant de fois qu'il faut pour appliquer complètement les conditions aux limites nécessaires, sans alourdir les calculs.

Le chapitre 4 est consacré à la validation de la méthode. Les premiers tests académiques présentés dans 4.1 montrent que la précision est tout à fait satisfaisante pour une formulation pénalisée du problème de contact. Les temps CPU sont augmentés par rapport à ceux obtenus pour les symétries planes, probablement à cause de la présence des plusieurs termes pénalisés dans les systèmes linéaires, mais la réduction de temps de calcul estimée par rapport à la simulation sur tout le domaine est considérable. Le test industriel offert par Ascoforge, présenté dans le chapitre 4.2, montre une bonne précision globale de l'algorithme durant toute la simulation, précision évaluée en mesurant l'écart entre une surface de symétrie et son image par rotation. Par ailleurs, ce test qui a une cinématique particulière met en évidence l'impossibilité de traiter ce type de problème en utilisant les symétries planes, même si le problème vérifiait effectivement des conditions de symétries planes. Dans le paragraphe 4.3, on présente un exemple de simulation de forgeage avec des outils déformables, ce qui montre la fiabilité globale de la méthode.

Comme cette première partie s'appuie sur le contact maître-esclave, la suite évidente de ce travail est d'améliorer cette formulation, dans la deuxième partie de la thèse. Le problème de cette approche est que dans les cas où le maître est discrétisé plus finement que le corps esclave la précision se dégrade, car il y a des nœuds en contact sans conditions aux limites (voir chapitre 3.1 de la deuxième partie).

Dans le chapitre 2 on présente le problème continu du contact, la formulation faible du problème et la discrétisation éléments finis.

Le chapitre 3 présente plusieurs algorithmes de contact proposés par la littérature. Sans entrer en détails, on montre que l'approche symétrique (3.2) conduit à une formulation sur contrainte du problème. Le raccord intégral (3.3) et les éléments mortier (3.4) donnent des bons résultats en 2D mais en 3D ils sont difficiles à appliquer et potentiellement chers en temps CPU.

Aussi, le chapitre 3.5 présente l'approche quasi-symétrique. Cette formulation est similaire à celle symétrique, mais les multiplicateurs de Lagrange sont calculés seulement sur la

surface esclave, et ils sont projetés sur la surface maître. Cette formulation nous permet d'éviter de sur-contraindre le problème. Au niveau discret, il y a toujours une distinction entre la surface maître et la surface esclave. On intègre l'équation de contact seulement sur la surface esclave, donc cette formulation reste dans le cadre maître-esclave, mais cette fois tous les nœuds des deux interfaces en contact imposent des conditions de contact qui leur sont associées. Le contact quasi-symétrique est implémenté dans le cadre d'une formulation nodale pénalisée.

Le chapitre 4 présente les diverses validations de cette méthode. En 4.1 on s'occupe d'évaluer la vitesse de convergence de cette méthode, en utilisant une famille de maillages emboîtés. La formulation quasi symétrique, ainsi que celle habituelle ont une bonne vitesse de convergence, similaire à celle obtenu avec des maillages coïncidents. En 4.2 on présente un patch test défini sur un maillage non régulier qui ne pose toujours pas de problèmes de consistance pour la formulation standard. Toutefois, en utilisant la formulation maître esclave, on double pratiquement la précision et on voit une amélioration nette du champs de pressions transmis. Le premier test du chapitre 4.3 accentue cette conclusion, et le deuxième test de cette section montre un net avantage en termes de précisions de la formulation quasi-symétrique quand le maillage du maître est plus raffiné que celui de l'esclave. En effet, ce test montre que la précision ne dépend quasiment pas du choix du maître de l'esclave. Le test d'indentation présente dans cette partie est un test extrême de détection du contact qui donne des résultats corrects quand on utilise le contact quasi symétrique, même s'il n'y a pas aucun nœud du corps esclave en contact.

Les cas d'étude industriels proposés par les partenaires de Simulforge sont regroupés dans le chapitre 5. Le première est le forgeage d'une pièce automobile constituée de deux matériaux en contact bilatéral collant et qui sont remaillés plusieurs fois au cours de la simulation du forgeage. Les calculs tournent pratiquement aussi vite avec la formulation quasi-symétrique qu'avec la que la version maître-esclave de base, mais à la fin de la simulation on obtient une bien meilleure qualité des résultats. Cette conclusion est confirmée par le deuxième test industriel, sur lequel on observe visuellement une meilleure distribution de la pression sur la zone en contact. Ces deux teste montrent aussi la stabilité et la fiabilité de l'implémentation.

### ***Conclusions et perspectives***

Les méthodes présentées dans cette thèse se montrent efficaces et fiables. Les symétries de répétition permettent de réduire considérablement le temps CPU pour la simulation du forgeage des engrenages hélicoïdaux, et l'approche quasi-symétrique du contact améliore la précision des simulations multi-corps, et rend le logiciel plus facile à utiliser.

En perspective, l'approche quasi-symétrique peut être utilisée aussi pour traiter les symétries de répétition. Le frottement est un problème encore ouvert. Quelques tests montrent qu'une approche symétrique du frottement donne des bons résultats, mais il est nécessaire d'une étude plus approfondie sur le sujet. Les deux méthodes présentées peuvent également être étendues à d'autres problèmes faisant apparaître ces types de symétries de répétition, comme le fluotournage, et à d'autres méthodes de résolution du contact, comme les formulations intégrées.

## **CONTENTS :**

<b>INTRODUCTION</b>	<b>1</b>
<b>PART 1 – HELICAL GEAR FORGING SIMULATION USING RECURRENT BOUNDARY CONDITIONS</b>	<b>5</b>
Abstract	7
1. INTRODUCTION	8
2. PROBLEM STATEMENT	9
2.1 Continuous problem	9
2.2 Discrete problem and Algorithm Splitting	13
3. RECURRENT BOUNDARY CONDITIONS	17
3.1 Recurrent condition	17
3.2 Discrete periodicity condition for velocities	18
3.3 Discrete periodicity conditions for temperatures	20
3.4 Node on the symmetry axis	20
3.5 Deformable tools	21
3.6 Algorithm for deformable tools	22
4. APPLICATIONS	24
4.1 Accuracy and time reduction evaluations	24
4.2 Industrial Test. Helical Gear Forging	28
4.3 Gear forging with deformable dies	31
5. CONCLUSIONS	35

<b>PART 2. A QUASI-SYMMETRIC CONTACT FORMULATION FOR LARGE 3D DEFORMATION SOLID MECHANICS</b>	37
ABSTRACT	39
1. INTRODUCTION	39
2. DEFORMABLE BODIES: CONTACT FORMULATIONS	40
2.1 Contact equations	40
2.2 Problem statement	41
2.3 Finite element discretization	42
3. CONTACT FORMULATIONS	43
3.1 Master / Slave	43
3.2 Double Pass	44
3.3 Integral joint	45
3.4 Mortar elements	47
3.5 Quasi-symmetric formulation	47
4. VALIDATIONS	49
4.1 Convergence rate	49
4.2 Contact patch test	52
4.3 Qualitative tests	55
4.6 Industrial forging problem	68
5. APPLICATONS	61
<b>CONCLUSION AND PROSPECTS</b>	67
<b>REFERENCES</b>	71

# **INTRODUCTION**



## 1. INTRODUCTION

### *General considerations*

The forging industry in Europe had a continuous growth during the last decade, even if the number of forging companies diminished. The companies involved in this competition have a constant need to increase the quality of the products and to decrease the production costs. The traditional design stages of a new product series imply expensive trials, on actual forging machines, which require stopping the production. The tendency is now to replace these tests by virtual, numerical ones. For the moment, the actual trials are not eliminated, but their number has considerably decreased. Using numerical simulation a wide range of mechanical and thermal data can be obtained, allowing the numerical optimization of the forging series, of the required forming energy, allowing to increase the tools life-span and making so possible to understand the reasons why a proposed design is not satisfactory or to improve the current one

Few years ago, numerical simulation was the domain of only few experts having a solid background in mechanics, numerical methods and programming. On the other hand, the computers were expensive and much slower. However, this situation is continuously changing, the computer prices are dropping and the performances are exploding. In the meantime, the software progressed, becoming more and more user-friendly and robust.

The first finite element based simulations took place in early seventies. At CEMEF, in 1981 the development of Forge2® started, for running forging simulations on axisymmetrical configurations. The studies for a fully 3D simulation code started in 1983, and in 1991 the first commercial version of Forge3® was launched. This software allows simulating forming processes with large deformations, such as forging, rolling, etc. It has a friendly interface, so numerical tests can be easily created and launched without requiring advanced knowledge of numerical methods. It provides the forming history undergone by the workpiece i.e. strain, stress, temperature, as well as global values such as forging force or energy, stresses on the tools, etc.

### *The frame of this work*

This thesis is a part of a larger project gathering several research laboratories called SIMULFORGE, sponsored by the French government. This project also puts together the efforts of 16 French forging companies, the Technical Center of Mechanical Industries (CETIM) and TRANSVALOR, a company in charged marketing Forge3®.

### *The objectives of the thesis*

The purpose of this study is twofold: reducing the required computational time for the forging simulation of helical gears by taking into account the non conventional symmetries of the problem, and improving the contact algorithm between deformable bodies, like the workpiece and the tools in the forging context.

When this research was started, an academic version of Forge3® was available, which was capable of running simulations for multiple bodies problems. The contact between deformable bodies was handled by a Master / Slave algorithm. This formulation was then used in the first part of this study, about the recurrent boundary conditions. So, the first part of this thesis, which is about to be published as an article in the Special Issue of the International Journal of Forming Processes 2004, presents the basics of Forge3®, and the proposed approach to handle this type of boundary conditions. The purpose is to allow running the forging simulation of helical gears (or any such repetitive configurations) only on one tooth of the domain, both for the workpiece and for the dies. The recurrent boundary conditions are regarded as the contact conditions between deformable bodies.

Therefore, after acquiring profound knowledge of the contact formulations and algorithms, the question of developing more symmetrical contact algorithms arose. This is the purpose of the second part of this thesis. Part 2 provides detailed description of the quasi-symmetrical contact formulation, and of the several tests, both academical and industrial that have been used to validate and evaluate this new formulation.

**PART 1. HELICAL GEAR FORGING  
SIMULATION USING RECURRENT  
BOUNDARY CONDITIONS**



---

# Helical gear forging simulation using recurrent boundary conditions

Sorin Popa<sup>1</sup>, Lionel Fourment<sup>1</sup>

<sup>1</sup> Cemef - Ecole des Mines de Paris & UMR CNRS n° 7635

B. P. 207, F-06904 Sophia Antipolis Cedex

URL: <http://www-cemef.cma.fr/>

e-mail: [lionel.fourment@ensmp.fr](mailto:lionel.fourment@ensmp.fr)

---

*ABSTRACT.* In gear forging simulation, the use of symmetries is obviously an efficient solution to reduce the computational time. However, for helical gears, standard plane symmetry conditions do not hold. They have to be extended to recurrent boundary conditions where the material flow that leaves one of the symmetry surface re-enters through the symmetric one, which is derived from it by a rotation of  $2\pi/N_{teeth}$  radians, ( $N_{teeth}$  is the number of teeth of the gear). In this case, the symmetry surfaces are not necessarily plane. This paper presents a master-slave algorithm for imposing these conditions, both for velocities and temperatures. It makes it possible to carry out simulations of helical gear forging considering only one tooth. Using a Lagrangian mesh, the symmetry surfaces are not steady during the deformation process, so a special treatment is required to handle the contact with deformable tools in the recurrent frame. Academic tests are studied to evaluate the accuracy of this approach, and then industrial applications show its robustness.

*KEYWORDS.* recurrent boundary conditions, master-slave algorithm, forging, helical gear, contact between deformable bodies

---

## 1. INTRODUCTION

Numerical simulation is an important step of the design process, particularly in forging where its cost is very low compared to industrial experiments. Actual trials require tools manufacturing and stopping industrial production, which all together results in high prices. Moreover, numerical simulation provides extensive information like material flow, tool stresses and life span or elastic spring back, information that are difficult to obtain otherwise. Therefore, it is a very attractive alternative. It also allows process optimisation in a very simple and friendly way, for instance to improve the tool geometries in order to decrease the required energy and increase the tooling life span. However, complex 3D simulations have a significant computational cost that has to be acknowledged and that may reduce its attractiveness. The purpose of this work is to reduce this computational cost for the simulation of helical gear forging (see figure 1) or similar processes, by reducing the problem size taking into consideration the natural symmetries of the process. In fact, it is theoretically possible to study only  $2\pi / N_{teeth}$  of the problem, where  $N_{teeth}$  is the number of teeth of the gear. These symmetries are not standard, like plane symmetries. Usually, they are not handled by finite element software, so the entire workpiece has to be considered, which results into very large computational time.



*Figure 1. Example of helical gears.*

As the process exhibits same symmetries as the gear itself, the material flow is periodic according to a rotation of  $2\pi / N_{teeth}$  along the gear axis. It allows considering the material volume of only one tooth. Some authors call this type of boundary conditions “principle of repeatability” or “cyclic symmetry” (Huang et al. 04), or qualify it as recurrent (Park et al. 97). With little modifications, this principle also applies to other types of recurrent boundary conditions, where, for instance, rotation is replaced by translation, as in the forming of a composite material at a micro scale. In (Park et al. 97), the method is presented in the limited frame of a structured mesh with nodes coinciding by rotation of the symmetry surfaces. In (Huang et al. 04), it is extended to unstructured meshes, without any constraint on the mesh, which makes it possible to apply it to both 2D and 3D problems. Here, the

same approach is followed, and is further extended to coupled calculations with deformable tools. This work is developed in the Forge3® finite element software that is based on a P1+/P1, velocity and pressure formulation (Aliaga et al. 98), uses unstructured meshes of tetrahedra and has automatic remeshing facilities (Coupez 94). Next section presents the thermo-mechanical problem and its finite element resolution. Section 3 introduces the recurrent boundary conditions in the frame of a master/slave contact algorithm between deformable bodies. Final section shows numerical simulations of complex gear forging, both with rigid and deformable tools.

## 2. PROBLEM STATEMENT

### 2.1. Continuous problem

The problem equations are presented in a rather simplified way for cold forging conditions. More details about the formulation and about more complex material models can be found in (Aliaga et al. 98, Barboza et al. 02, Pichelin et al. 01). The Prandl Reuss additive decomposition of the strain rate tensor  $\dot{\boldsymbol{\epsilon}}$  is considered:

$$\begin{cases} \dot{\boldsymbol{\epsilon}} = \dot{\boldsymbol{\epsilon}}^{el} + \dot{\boldsymbol{\epsilon}}^{vp} \\ \dot{\boldsymbol{\epsilon}}^{el} = \mathbf{L}^{-1}\dot{\boldsymbol{s}} \end{cases} \quad [1]$$

where  $\dot{\boldsymbol{\epsilon}}^{el}$  is the elastic part of the strain rate tensor and  $\dot{\boldsymbol{\epsilon}}^{vp}$  the viscoplastic one,  $\boldsymbol{\sigma}$  is the stress tensor and  $\dot{\boldsymbol{\sigma}}$  its time derivative,  $\mathbf{L}$  is a 9x9 tensor containing the Lamé coefficients  $\lambda$  and  $\mu$  :

$$\dot{\boldsymbol{s}} = 2\mu\dot{\boldsymbol{\epsilon}} + \lambda tr(\dot{\boldsymbol{\epsilon}})\mathbf{I} \quad [2]$$

The viscoplastic deformation follows the Norton-Hoff constitutive model. Considering  $K$ , the material consistency and  $m$ , the strain rate sensitivity coefficient, we have:

$$\boldsymbol{s} = \boldsymbol{s} + p\mathbf{I} = 2K(\sqrt{3}\dot{\boldsymbol{\epsilon}})^{m-1}\dot{\boldsymbol{\epsilon}}^{vp} \quad [3]$$

$$tr(\dot{\boldsymbol{\epsilon}}^{vp}) = 0 \quad [4]$$

$$\text{div}(\mathbf{v}) = -\frac{3(1-2\nu)}{E} p \quad [5]$$

where  $\mathbf{s}$  is the deviatoric stress tensor,  $E$  the Young coefficient,  $\nu$  the Poisson coefficient,  $\dot{\bar{\epsilon}}$  the equivalent strain rate, and  $p$  the hydrostatic pressure:

$$p = -\frac{1}{3} \text{tr}(\mathbf{s}) \quad \text{and} \quad \dot{\bar{\epsilon}} = \sqrt{\frac{2}{3} (\dot{\epsilon}^{vp} : \dot{\epsilon}^{vp})} \quad [6]$$

Neglecting all external forces like gravity and inertia, at any time of the process, the balance and heat equations are written as:

$$\text{div}(\mathbf{s}) = 0 \quad [7]$$

$$\rho c_p \frac{dT}{dt} + \text{div}(k \cdot \text{grad}(T)) = f \mathbf{s} : \dot{\epsilon} \quad [8]$$

where  $T$  is the temperature,  $c_p$  the heat capacity,  $k$  the conductivity,  $\rho$  the density and  $f$  is a conversion rate between 0 and 1 (usually around 0.9).

### 2.1.1 Contact with rigid tools

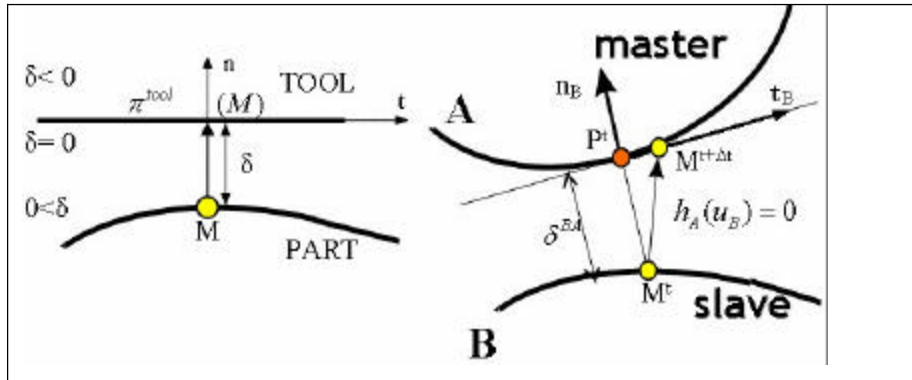


**Figure 2.** a) Contact with rigid tool      b) Contact between deformable bodies

These equations are complemented by different boundary conditions, such as unilateral contact with the forming tools, or Signorini conditions. Considering  $\langle \cdot \rangle$  as the scalar product, these conditions are written as:

$$\text{on } \partial\Omega_{\text{contact}}, \begin{cases} (\mathbf{u} - \mathbf{u}_{\text{tool}}) \cdot \mathbf{n} \leq \delta \\ \mathbf{s}_n = \mathbf{s} \mathbf{n} \cdot \mathbf{n} \leq 0 \\ [(\mathbf{u} - \mathbf{u}_{\text{tool}}) \cdot \mathbf{n} - \delta] \sigma_n = 0 \end{cases} \quad [9]$$

where  $\mathbf{u}$  is the displacement vector,  $\mathbf{u}_{\text{tool}}$  is the tool one,  $\mathbf{n}$  is the ingoing normal of the tool surface,  $\sigma_n$  is the normal stress vector, and  $\delta$  is the signed distance to the tool surface (which is negative inside the tool, see figure 2.a). For the contact conditions, displacement unknowns are used while velocity unknowns are preferred elsewhere. Several models can be used for the friction boundary conditions between the workpiece and the rigid tools. Neglecting the gliding threshold, equation [10] gives the Tresca model:

$$\text{on } \partial\Omega_{\text{friction}}, \boldsymbol{\tau} = -m \frac{-\sigma_0}{\sqrt{3}} \frac{\Delta \mathbf{v}_t}{\|\Delta \mathbf{v}_t\|} \quad [10]$$

$$\boldsymbol{\tau} = \mathbf{s} \mathbf{n} - s_n \mathbf{n} \quad [11]$$

$$\Delta \mathbf{v}_t = \mathbf{v} - \mathbf{v}_{\text{tool}} - ((\mathbf{v} - \mathbf{v}_{\text{tool}}) \cdot \mathbf{n}) \mathbf{n} \quad [12]$$

where  $\boldsymbol{\tau}$  is the tangential component of the stress tensor on the contact surface,  $\Delta \mathbf{v}_t$  is the relative tangent velocity between the bodies,  $\bar{m}$  is the friction coefficient and  $\sigma_0$  is the material flow stress.

### 2.1.2 Contact between deformable bodies

The contact conditions between two deformable bodies  $A$  and  $B$  (workpiece and deformable tool, for example) are given in [13] when body  $B$  is in contact with body  $A$ :

$$\text{on } \partial O_{AB}, \begin{cases} h_A(\mathbf{u}_B) = (\mathbf{u}_B - \mathbf{u}_A) \cdot \mathbf{n}_B - \delta^{BA} \leq 0 \\ \sigma_n = s_A \mathbf{n}_A \cdot \mathbf{n}_A = s_B \mathbf{n}_B \cdot \mathbf{n}_B \leq 0 \\ [\sigma_n] h_A(\mathbf{u}_B) = 0 \end{cases} \quad [13]$$

and also, symmetrically, the inequality  $h_B(\mathbf{u}_A) \leq 0$  could be considered. These equations can be extended to any number of bodies. The friction condition between bodies  $B$  and  $A$  is written similarly to [10], with:

$$\Delta \mathbf{v}_t = (\mathbf{v}_B - \mathbf{v}_A) - ((\mathbf{v}_B - \mathbf{v}_A) \cdot \mathbf{n}_B) \mathbf{n}_B \quad [14]$$

As for the contact conditions, the friction equation could also be written for the body  $A$  with body  $B$ . In anticipation to the equations that will be necessary to handle the recurrent boundary conditions, we introduce here the bilateral sticking contact equations between deformable bodies:

$$h_A(\mathbf{u}_B) = \mathbf{u}_B - \mathbf{u}_A - \delta^{BA} \mathbf{n}_B = 0 \quad [15]$$

These boundary conditions are completed with the free surface one:

$$\text{on } \partial\Omega_{free}, \quad \mathbf{s} \mathbf{n} = 0 \quad [16]$$

### 2.1.3 Thermal boundary conditions

For the thermal problem, several boundary conditions are applied. Considering  $h_{ex}$  the convection/radiation coefficient with the air,  $h_{tool}$  the transfer coefficient with a rigid tool,  $T_{ex}$  the air temperature and  $T_{tool}$  the rigid die temperature, the convection/radiation boundary conditions are written as:

$$\text{on } \partial\Omega_{free}, \quad -k \text{grad}(T) \cdot \mathbf{n} = h_{ex}(T - T_{ex}) \quad [17]$$

and a similar equation describes the heat exchange with a rigid tool:

$$\text{on } \partial\Omega_{contact}, \quad -k \text{grad}(T) \cdot \mathbf{n} = h_{tool}(T - T_{tool}) \quad [18]$$

Considering  $h_c$  the conductivity of the interface, the heat transfer between two deformable bodies is given by:

$$-k_B \text{grad}(T_B) \cdot \mathbf{n} = h_c(T_B - T_A) \quad \text{and} \quad -k_A \text{grad}(T_A) \cdot \mathbf{n} = h_c(T_A - T_B) \quad [19]$$

The heat produced by the friction is also considered:

$$\text{on } \partial\Omega_{friction}, \quad -k \text{grad}(T) \cdot \mathbf{n} = h_{friction} \mathbf{t} \cdot \mathbf{v} \quad [20]$$

where  $h_{friction}$  is a coefficient depending on the effusivities of the two parts in contact.

### 2.1.4 Plane symmetry

Considering  $\mathbf{n}_{sym}$  the outgoing normal of the symmetry plane  $\partial\Omega_{sym}$ , the following symmetry boundary conditions are imposed respectively for the mechanical and thermal problems:

$$\text{on } \partial\Omega_{sym}, \mathbf{v} \cdot \mathbf{n}_{sym} = 0 \quad [21]$$

$$-k(\text{grad}(T)) \cdot \mathbf{n}_{sym} = 0 \text{ on } \partial\Omega_{sym} \quad [22]$$

## 2.2. Discrete problem and algorithm splitting:

### 2.2.1 Time discretization

Using an updated Lagrangian formulation, an explicit Euler time discretization scheme is chosen for the mechanical problem. Considering  $x^t$  the values at time  $t$ , the values at time  $t + \Delta t$  can be approximated by:

$$\mathbf{x}^{t+\Delta t} = \mathbf{x}^t + \mathbf{v}^{t+\Delta t} \Delta t \quad [23]$$

Using this time discretization, the contact boundary conditions are written again at time  $t + \Delta t$  using velocities unknowns [24], so the unilateral contact with the rigid tools is given by [25].

$$\mathbf{u}^{t+\Delta t} = \mathbf{x}^{t+\Delta t} - \mathbf{x}^t = \mathbf{v}^{t+\Delta t} \Delta t \quad [24]$$

$$(\mathbf{v}^{t+\Delta t} - \mathbf{v}_{tool}^{t+\Delta t}) \cdot \mathbf{n}^t - \frac{\delta^t}{\Delta t} \leq 0 \quad [25]$$

Similarly, the bilateral sticking contact condition is given by:

$$\mathbf{v}^{t+\Delta t} - \mathbf{v}_{tool}^{t+\Delta t} - \frac{\delta^t}{\Delta t} \mathbf{n}^t = 0 \quad [26]$$

From now on, the distances  $d$  and  $d^{BA}$  as well as the normals  $n$  and  $n_b$  are calculated at time  $t$ , so the time indexes are not written any longer. Then, the bilateral sticking and the unilateral contact equations between deformable bodies respectively become:

$$h_A(\mathbf{u}_B) = \mathbf{v}_B^{t+\Delta t} - \mathbf{v}_A^{t+\Delta t} - \frac{\delta^{BA}}{\Delta t} \mathbf{n}_B = 0 \quad [27]$$

$$h_A(\mathbf{u}_B) = (\mathbf{v}_B^{t+\Delta t} - \mathbf{v}_A^{t+\Delta t}) \cdot \mathbf{n}_B - \frac{\delta^{BA}}{\Delta t} \leq 0 \quad [28]$$

Concerning the thermal problem, a time discretization scheme with two time steps is used. Without going too much into details, the thermal problem is solved at an intermediate time  $t_i \in [t, t + \Delta t]$  and:

$$\frac{dT^{t_i}}{dt} = (1-\gamma)\frac{T^t - T^{t-\Delta t}}{\Delta t} + \gamma\frac{T^{t+\Delta t} - T^t}{\Delta t} \quad [29]$$

The temperature at time  $t + \Delta t$  are updated using the following equation:

$$T^{t+\Delta t} = \frac{T^{t_i}}{\alpha_3} - (\alpha_1 T^{t+\Delta t} + \alpha_2 T^t) \quad [30]$$

where the numerical coefficients  $\alpha_1, \alpha_2, \alpha_3, \gamma$  are given by the Dupont scheme ( $\alpha_1 = \frac{1}{4}, \alpha_2 = 0, \alpha_3 = \frac{3}{4}, \gamma = 1$ ).

Considering an elasto-viscoplastic material, and  $(v^t, p^t, T^t, \Omega^t)$  being known, the resolution of the thermo-mechanical problem provided by equations [7], [5], [8] and previously described boundary conditions, allows calculating  $(v^{t+\Delta t}, p^{t+\Delta t}, T^{t+\Delta t}, \Omega^{t+\Delta t})$ . The mechanical and thermal problems are coupled, as the consistency of the material depends on the temperature, and the heat equation depends on the mechanical solution. A splitting algorithm is used, so the thermo-mechanical problem is decomposed in a mechanical problem that uses the temperature field of the previous time step, and a thermal problem that uses the calculated mechanical solution.

### 2.2.2 Finite element formulation

Considering  $H_{\Omega^t}^1$  a Sobolev space on  $\Omega^t$ , and  $L_{\Omega^t}^2$  a Hilbert space on  $\Omega^t$ , the space of kinematically admissible velocities is defined as:

$$V^{CA} = \left\{ \begin{array}{l} \mathbf{v} = (\mathbf{v}_A, \mathbf{v}_B) \in H_{\Omega_A^t}^1 \times H_{\Omega_B^t}^1, h_A(\mathbf{v}_B) \leq 0 \text{ on } \partial\Omega_{AB}, \\ (\mathbf{v} - \mathbf{v}_{tool}) \cdot \mathbf{n} - \frac{\delta}{\Delta t} \leq 0 \text{ on } \partial\Omega_{contact}, \mathbf{v} \cdot \mathbf{n}_{sym} = 0 \text{ on } \partial\Omega_{sym} \end{array} \right\}$$

and the one of the kinematically admissible to 0 as:

$$V_0^{CA} = \left\{ \begin{array}{l} \mathbf{v}^t = (\mathbf{v}_A^t, \mathbf{v}_B^t) \in H_{\Omega_A^t}^1 \times H_{\Omega_B^t}^1, \mathbf{v}_B^t \cdot \mathbf{n}_B \leq 0 \text{ on } \partial\Omega_{AB}, \\ \mathbf{v}^t \cdot \mathbf{n} \leq 0 \text{ on } \partial\Omega_{contact}, \mathbf{v}^t \cdot \mathbf{n}_{sym} = 0 \text{ on } \partial\Omega_{sym} \end{array} \right\}$$

Considering  $P = (L^2_{\Omega'_t}, L^2_{\Omega'_b})$ , the variational formulation of the mechanical problem becomes:

$$\left\{ \begin{array}{l} \text{Find } (\mathbf{v}^{t+\Delta t}, p^{t+\Delta t}) \in (V^{CA}, P), \text{ s.t :} \\ \forall \mathbf{v}^* \in V_0^{CA}, \sum_{b=A,B} \left\{ \int_{\Omega_b} \mathbf{s}_b^{t+\Delta t} : \dot{\mathbf{e}}^* dw - \int_{\Omega_b} p_b^{t+\Delta t} \text{div}(\mathbf{v}^*) dw - \int_{\partial\Omega_b^{\text{friction}}} \mathbf{t}_b^{t+\Delta t} \cdot \mathbf{v}_{tb}^* dS \right\} - \\ \int_{\partial\Omega_B^{\text{friction}}} \mathbf{t}_B^{t+\Delta t} \cdot \mathbf{v}_{tB}^* dS = 0 \\ \forall p^* \in P, \sum_{b=A,B} \left\{ \int_{\Omega_b} \text{div}(\mathbf{v}_b^{t+\Delta t}) \cdot p^* dw - \int_{\Omega_b} p^* \frac{3(1-2\nu)}{E} \frac{p_b^{t+\Delta t} - p_b^t}{\Delta t} dw \right\} = 0 \end{array} \right. \quad [31]$$

The variational form of the thermal problem is written as:

$$\left\{ \begin{array}{l} \int_{\Omega_b} \rho c_p \frac{dT}{dt} T^* dw + \int_{\Omega_b} k \nabla T \cdot \nabla T^* dw + \int_{\Omega_b^{\text{contact}}} h_{\text{tool}} (T - T_{\text{tool}}) \cdot \nabla T^* dS + \\ \sum_{b=A,B} \left\{ \int_{\Omega_b^{\text{free}}} h_{\text{ex}} (T - T_{\text{ex}}) \cdot \nabla T^* dS - f \int_{\Omega_b} \mathbf{s} : \dot{\mathbf{e}} T^* dw + \int_{\Omega_b^{\text{friction}}} h_{\text{friction}} \mathbf{t}_B \cdot \mathbf{v}_B T^* dS \right\} \\ + \int_{\partial\Omega_{AB}} h_C (T_B - T_A) \cdot \nabla T^* dS + \int_{\partial\Omega_{AB}^{\text{friction}}} h_{AB} \mathbf{t}_B \cdot \mathbf{v}_B T^* dS = 0 \end{array} \right. \quad [32]$$

### 2.2.3 Space discretization

For space discretization, an unstructured mesh of tetrahedra is used with a P1+/P1 velocity/pressure interpolation, and a P1 interpolation for the temperature (Aliaga et al. 98):

$$\left\{ \begin{array}{l} X(\zeta) = \sum_{n=1}^{Nbn} X_n N_n(\zeta), \quad V(\zeta) = \sum_{n=1}^{Nbn} V_n N_n(\zeta) + \sum_{e=1}^{Nelts} V_e \Phi_e(\zeta) = V_l + V_b, \\ P(\zeta) = \sum_{n=1}^{Nbn} P_n N_n(\zeta), \quad T(\zeta) = \sum_{n=1}^{Nbn} T_n N_n(\zeta) \end{array} \right. \quad [33]$$

where  $X$  are the coordinates of a material point in a global reference system,  $Nbn$  is the number of nodes of the mesh,  $Nelts$  is the number of elements,  $\zeta$  are the local

coordinates of  $X$ ,  $N_n$  the linear interpolation function at node  $n$  and  $\Phi_e$  the “bubble” interpolation function of element  $e$ .

### 2.2.4 Contact between deformable bodies

In the previous set of equations, the contact between deformable bodies is treated with a master-slave formulation, as presented in (Barboza et al. 02, Pichelin et al. 01), and using “contact” elements. Considering  $B$  as the slave body and  $A$  as the master one, the contact conditions [25] or [26] are only enforced for the slave body, in order to avoid writing an over-constrained problem (Barboza et al. 02). A contact element consists of a node  $k$  of the slave body  $B$  and a triangular facet  $f_A^k$  of the master surface  $\partial\Omega_A$  that contains the orthogonal projection  $\pi^A(k)$  of  $k$  on the master body (see figure 3). Using a nodal contact formulation, the contact equation becomes:

$$\forall k \in \partial\Omega_B^{contact}, h_A(V_k) = (V_k - V_{p^A(k)}) \cdot \mathbf{n}_B^k - \frac{\delta_k^{BA}}{\Delta t} \leq 0 \quad [34]$$

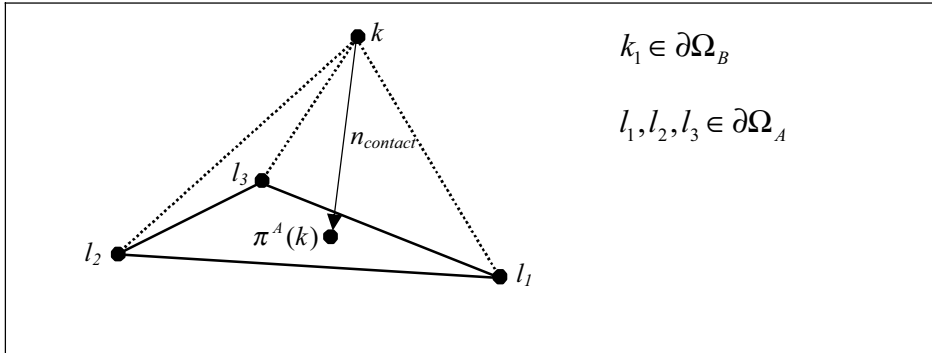


**Figure 3.** Contact element.

The velocity of  $\pi^A(k)$  is obtained by a linear interpolation on  $f_A^{(k)}$ .

$$V_{p^A(k)} = \sum_{l \in f_A^k} N_l^{\partial\Omega_A}(\zeta_A^k) \cdot V_l \quad [35]$$

Using a penalty formulation to enforce the contact equations, the following potential is introduced:

$$\begin{aligned}
 \Phi_{cont} = & \frac{1}{2} \sum_{k \in \partial\Omega_{AB}} \rho S_k \left[ \left( \mathbf{V}_k - \sum_{l \in f_A^k} N_l^{\partial\Omega_A}(\xi_A^k) \mathbf{V}_l \right) \cdot \mathbf{n}_B^k - \frac{\delta_k^{BA}}{\Delta t} \right]^{+2} \\
 & + \frac{1}{2} \sum_{b=A,B} \sum_{k \in \partial O_b^{contact}} S_k \left[ (\mathbf{V}_k - \mathbf{v}_{tool}) \cdot \mathbf{n}^k - \frac{\delta_k}{\Delta t} \right]^{+2}
 \end{aligned} \tag{36}$$

where  $\rho$  is the penalty coefficient,  $[x]^+ = \frac{x + |x|}{2}$  is the positive part function,  $N^{\partial\Omega_A}$  are the linear interpolation functions on the surface elements (triangles) of body  $A$ , and  $S_k$  is a weighting coefficient which is equal to the averaged surface affected to

$$\text{node } k: S_k = \int_{\partial\Omega_b} N_k^{\partial\Omega_b} ds$$

For each node  $k$  of the slave body, the distances  $\delta_{AB}^k$ , the facet  $f_A^k$  and the coordinates of the projection  $\xi_A^k$ , are calculated by a contact algorithm that uses the 2D “skin” of the master body as a fictitious tool (Barboza et al. 02). A correspondence between the nodes  $l_{tool}$  of this fictitious tool and the nodes  $l_A$  of the master body is used to build the contact elements and to apply the boundary conditions [34]. By the differentiation of equation [36], the contributions to the gradient and Hessian matrixes are obtained. The set of the deformable bodies is handled like a single domain. The resulting global non linear system of mechanical equations is solved by a Newton-Raphson algorithm. The linear systems so generated are solved by a Preconditioned Conjugate Residual iterative method. In order to avoid element degeneration, an automatic remeshing algorithm (Coupez 94) is used. It can be triggered by several criteria, such as element quality, tool penetration, excessive incremental deformation, or remeshing period established by the user. The transfer of values from the initial mesh onto the new one is tackled using a P1 interpolation. The remeshing and transfer procedures are applied separately on each body (Barboza et al. 02).

### 3. RECURRENT BOUNDARY CONDITIONS

#### 3.1. Recurrent conditions

The recurrent condition makes its possible to consider only  $1/N_{teeth}$  part of the workpiece, where  $N_{teeth}$  is the number of teeth of the helical gear. In fact, any material point  $A$  of the workpiece flows in the same way as the corresponding point  $B$  that is derived by rotation  $R$  with the angle  $\phi = \frac{2\pi}{N_{teeth}}$  (see figure 4).  $\bar{R}$

denotes the rotation matrix of coordinates while  $R$  denotes its vectorial counterpart that is used for vectors. When considering only one tooth of the gear, the two symmetry (or recurrent) surfaces correspond each other by rotations  $\bar{R}$  and  $'R$ . They are referred as  $S_A$  and  $S_B$  (see figure 4). This condition holds for any material point of the considered portion of the workpiece  $S_B$ . So, the recurrent boundary conditions are written as:

$$\forall x_B \in S_B, \exists x_A \in S_A \text{ s.t. } x_B = \bar{R}x_A, \text{ then } \begin{cases} \mathbf{v}(x_B) = \mathbf{R}\mathbf{v}(x_A) \\ T(x_B) = T(x_A) \end{cases} \quad [37]$$

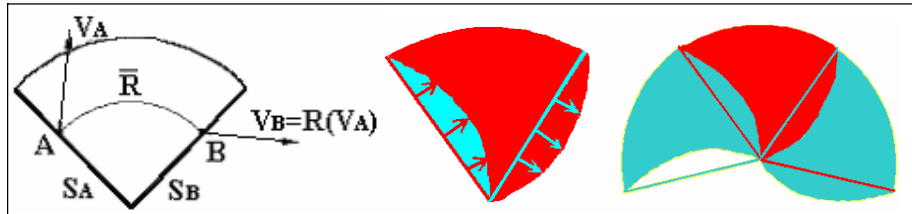


**Figure 4.** Basic recurrent condition: symmetry (recurrent) surfaces. Lagrangian approach.

### 3.2. Discrete recurrent conditions for velocities

At a discrete level, these conditions are applied to any node of the symmetry face  $S_B$ . Two different approaches are possible:

#### 3.2.1 Coincident meshes

Using coincident meshes, either with structured or unstructured grids, the problem is perfectly symmetric: equation [37] is exactly applied to the finite element nodes. This method is described in (Park et al. 97) and used in (Huang et al. 04) for 2D applications. However, it is difficult to implement because the meshes should be kept perfectly coincident any time increment, so requiring to use a special mesh generator to maintain the coincidence of nodes. As in (Huang et al. 04), a more simple approach that does not require introducing this constraint is preferred here.

#### 3.2.2 Non-coincident meshes

This approach is more compatible with the existing software, its Lagrangian formulation (see figure 4) and its remeshing algorithm. It consists in applying the conditions [37] at a discrete level, and in considering the projection  $\pi^{S_A}$  of any node of the symmetry face  $S_B$  onto the symmetry face  $S_A$ , such that:

$$\forall k \in S_B, \text{ if } \tilde{\mathbf{X}}_k = \rho^{S_A}(\bar{\mathbf{R}} \cdot \mathbf{X}_k) \text{ then : } \begin{cases} \mathbf{V}_k = \mathbf{R} \cdot \mathbf{V}(\tilde{\mathbf{X}}_k) \\ T_k = T(\tilde{\mathbf{X}}_k) \end{cases} \quad [38]$$

The symmetry (or recurrent) surfaces  $S_A$  and  $S_B$  play symmetric roles, so an equation symmetric to equation [38] should also be written. However, it is noticed that the condition [38] is very similar to a bilateral sticking contact condition between two deformable bodies [15, 27]. It is not possible, at the discrete level, both to prevent body  $A$  to penetrate body  $B$ , and body  $B$  to penetrate body  $A$ . It would result into an over-constrained problem (Barboza et al. 02, Bathe et al. 01, Pichelin et al. 01). Therefore, as for the contact between deformable bodies, a master / slave approach is used. The recurrent boundary condition [38] is only enforced for surface  $S_B$ . It is necessary to calculate the coordinates  $\tilde{\mathbf{X}}_k$  of the corresponding point of any node  $k$  of  $S_B$ , and to interpolate the velocities  $\mathbf{V}(\tilde{\mathbf{X}}_k)$  at this point [39].  $\tilde{f}_k$  represents here the facet of  $S_A$  that contains  $\tilde{\mathbf{X}}_k$ , and  $\tilde{\xi}_A^k$  the projection coordinates of the rotation of node  $k$ :

$$\forall k \in S_B, \mathbf{X}_h(\tilde{\mathbf{X}}_k) = \sum_{l \in \tilde{f}_k} \mathbf{X}_l N^l(\tilde{\xi}_A^k) \text{ and } \mathbf{V}(\tilde{\mathbf{X}}_k) = \sum_{l \in \tilde{f}_k} \mathbf{V}_l N^l(\tilde{\xi}_A^k) \quad [39]$$

Due to numerical errors,  $\tilde{\mathbf{X}}_k$  can be slightly different from  $\bar{\mathbf{R}}\mathbf{X}_k$ . So,  $\tilde{\delta}^k$ , the signed distance between  $\tilde{\mathbf{X}}_k$  and  $\bar{\mathbf{R}}\mathbf{X}_k$ , and  $\tilde{\mathbf{n}}^k$ , the outgoing normal of  $S_A$  in  $\tilde{\mathbf{X}}_k$ , has to be taken into account. The discrete boundary condition [38] is written again as follows:

$$\forall k \in S_B, \mathbf{V}_k - \mathbf{R}\mathbf{V}(\tilde{\mathbf{X}}_k) - \frac{\tilde{\delta}^k}{\Delta t} \mathbf{n}^k = 0 \quad [40]$$

Similarly to the bilateral sticking contact, the recurrent symmetry condition is imposed using a penalty method. The corresponding functional is written as:

$$\Phi = \sum_{k \in S_B} \frac{1}{2} \rho_{sym} S_k \left\| \mathbf{V}_k - \mathbf{R}\mathbf{V}(\tilde{\mathbf{X}}_k) - \frac{\tilde{\delta}^k}{\Delta t} \mathbf{n}^k \right\|^2 \quad [41]$$

where  $\rho_{sym}$  is the penalty coefficient for these conditions.

The contact algorithm that has been developed for handling the contact between a 3D mesh and a tool defined by a 2D mesh (see section 2), can also be used here. Surface  $S_A$  (see figure 5.b) is automatically created by considering the intersection between the part and its image after rotation (see figure 5.a). The ‘‘skin’’ of the

master surface  $S_A$  is first extracted and then rotated around the symmetry axis using the  $\bar{R}$  matrix. The rotated 2D mesh (see figure 5.c) is regarded as a tool (contact obstacle) in the contact algorithm, so providing the distance  $\tilde{\delta}^k$ , the normal  $\tilde{n}^k$ , and the interpolation factors for any node of  $S_B$ .

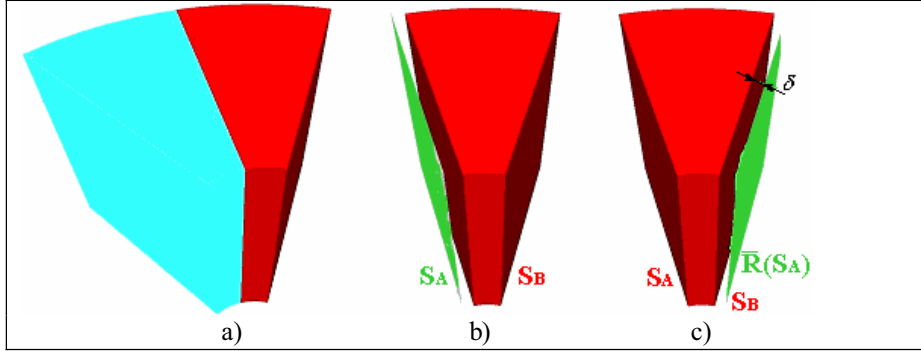


**Figure 5.** Fictitious tools creation: a) identification of the  $S_A$  surface, b) extraction of  $S_A$  surface, c) after rotation,  $\bar{R}S_A$  is regarded as a tool for the contact analysis of the nodes of  $S_B$ .

### 3.3. Discrete recurrent conditions for temperatures

For the temperature field  $T$ , at the discrete level, the recurrent boundary conditions are also formulated within a master / slave framework, which yields:

$$\forall k \in \partial\Omega_B, T_k = T(\tilde{X}_k) = \sum_{l \in \tilde{J}_k} T_l N^l(\tilde{\zeta}_A^k) \quad [42]$$

This equation is imposed using a penalty formulation, which functional is given by [43], where  $\rho_{ther}$  is a penalty coefficient:

$$\Phi_T = \sum_{k \in S_B} \frac{1}{2} \rho_{ther} S_k [T_k - T(\tilde{X}_k)]^2 \quad [43]$$

### 3.4. Specificity of the symmetry axis

Similarly to the situation of plane symmetries nodes, any node  $k_{axis}$  belonging to the symmetry axis cannot leave it. These nodes are eliminated from the symmetry

surface  $S_B$  and two successive conditions are applied to prevent their displacements in a plane perpendicular to the symmetry axis:

$$v_{k_{axis}} \cdot n_{sym1} = 0 \quad , \quad v_{k_{axis}} \cdot n_{sym2} = 0 \quad [44]$$

where:  $n_{sym1} \perp n_{axis}$ ,  $n_{sym2} \perp n_{axis}$  and  $n_{sym1} \perp n_{sym2}$

For the thermal problem, the nodes of the symmetry axis being eliminated from the symmetry surfaces, no heat exchange with the environment is allowed:

$$k(\text{grad}(T_{k_{axis}})) \cdot n_{sym1} = 0 \quad , \quad k(\text{grad}(T_{k_{axis}})) \cdot n_{sym2} = 0 \quad [45]$$

### 3.5. Deformable tools

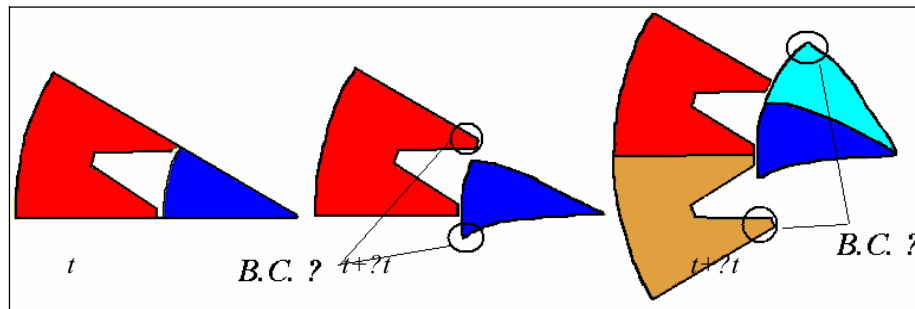


**Figure 6.** Periodicity conditions for problems with deformable tools. One portion of tool and workpiece at time  $t$ . Loss of correspondence at time  $t+\Delta t$ . Same loss of correspondence at time  $t+\Delta t$  with two portions of each.

One of the objectives of the finite element simulation of gear forging is to produce net-shape parts, so the coupled elastic deformation of the dies must be considered, following the method presented in (Barboza et al. 02, Pichelin et al. 01). For helical gears, it is important to take into account the recurrent boundary conditions [40] and [42], both for the workpiece and for the dies. However, because a Lagrangian approach is been used, the symmetry surfaces  $S_A$  and  $S_B$  are not steady (see figure 6) and their deformations follow the ones of the material flow. When using rigid dies, it is often necessary to discretize more than one tooth of the die in order to impose the proper boundary conditions, because very often the workpiece material flows into more than one tooth of the tool (see figures 6, 13, 16, 17). When using deformable dies, these deformations are not the same for the workpiece and for the dies (see last two examples of section 4). Therefore, it is virtually impossible to carry out the

simulation with only one tooth. Adding another “tooth” for the tool (yellow in figure 6) and for the workpiece (light blue in figure 6) does not help. In fact, there is still a region of the workpiece and a region of the tool without any boundary conditions (see figure 6). In order to avoid this, which would prevent us from using the recurrent boundary conditions with deformable tools, more tricky boundary conditions must be introduced.

### 3.6. Algorithm for deformable tools

The surface  $\partial\Omega_{tool}$  of the deformable tool is regarded as the master surface for the contact algorithm with the workpiece (see section 2). In order to make it possible to also detect the contact in a “void” area, in which it is not desired to actually compute the tool deformation, the surface of the tool is first duplicated and then rotated by the  $\bar{R}$  rotation. So, it produces a “ghost” surface  $\partial\Omega_{ghost}$  (see figure 7) in this “void” area. During this rotation, the correspondence of nodes between the initial and rotated tools is saved for the contact analysis. This construction of “ghost” surfaces can be repeated as many times as necessary, for instance, if the material is expected to flow into more than 3 teeth of the tools. Figure 7 shows only one “ghost” surface, while figure 8 provides a 3D example with two “ghost” surfaces on each side.

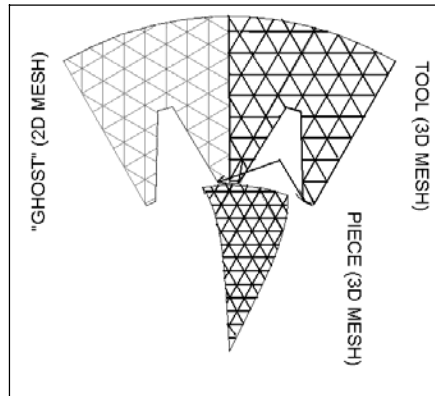


**Figure 7.** Deformable tools. Creation of a “ghost” surface  $\partial\Omega_{ghost}$  of the tool. Section view of a meridian plane of the symmetry axis.

Let us consider a node  $k$  of the workpiece surface that is in contact with  $\partial\Omega_{ghost}$  and denote by  $\bar{X}'_k$  the orthogonal projection of  $X_k$  onto it:  $\bar{X}'_k = \pi^{ghost}(X_k)$ . Let us also consider  $\bar{f}_k$  the facet of  $\partial\Omega_{ghost}$  that contains  $\bar{X}'_k$ :

$$\bar{X}'_k = \sum_{l' \in \bar{f}'_k} X_{l'} N_{l'}^{ghost}(\bar{\xi}'_k) \quad [46]$$

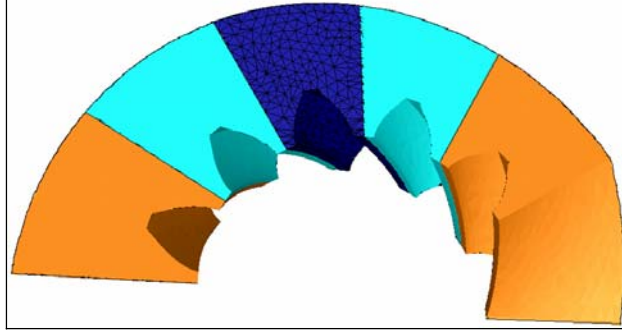


**Figure 8.** Initial surface mesh (in the centre) and ghost meshes for the contact analysis: two “ghosts” on each side of the initial mesh.

According to the construction process of  $\partial\Omega_{ghost}$ , there is a facet  $f_k$  of the original tool surface mesh that corresponds to  $\bar{f}'_k$ , such that:

$$\forall l' \in \bar{f}'_k, \exists l \in f_k, \text{ s.t. } X_{l'} = \bar{R} \cdot X_l \quad \text{and} \quad \bar{X}'_k = {}^t\bar{R} \bar{X}'_k = \sum_{l \in f_k} X_l N_{l'}^{ghost}(\bar{\xi}'_k) \quad [47]$$

Therefore:

$$V(\bar{X}'_k) = \mathbf{R} \cdot V(\bar{X}_k) = \mathbf{R} \cdot \left( \sum_{l \in f_k} V_l N_{l'}^{ghost}(\bar{\xi}'_k) \right), \quad T(\bar{X}'_k) = \sum_{l \in f_k} T_l N_{l'}^{ghost}(\bar{\xi}'_k) \quad [48]$$

So, the contact boundary conditions for the “void” regions become:

$$(V_k - V(\bar{X}'_k)) \cdot \mathbf{n}^k - \frac{\delta^k}{\Delta t} \leq, \quad 0T_k = T(\bar{X}'_k) \quad [49]$$



$$err_{mech\_rel} = \frac{\sum_{k \in S_B} \|V_k - RV(\tilde{X}_k)\|}{\sum_{k \in S_B} V_k} \quad \text{and} \quad err_{mech\_max} = \max_{k \in S_B} (\|V_k - RV(\tilde{X}_k)\|) \quad [50]$$

	MECHANICAL			THERMAL		
$\rho_{sym}$ $\rho_{ther}$	Nb of iterations for resolution	$err_{mech\_rel}$	$err_{mech\_max}$ [mm/s]	Nb of iterations for resolution	$err_{therm\_rel}$	$err_{therm\_max}$ [°C]
1				32	$1.6 \cdot 10^{-3}$	6.23
10	700	$1.1 \cdot 10^{-5}$	$4.0 \cdot 10^{-4}$	55	$2.4 \cdot 10^{-4}$	0.81
50	1000	$2.0 \cdot 10^{-6}$	$8.0 \cdot 10^{-5}$	104	$5.0 \cdot 10^{-5}$	0.16
100	1500	$1.1 \cdot 10^{-6}$	$4.2 \cdot 10^{-5}$	123	$2.5 \cdot 10^{-5}$	0.08
500	2600	$2.3 \cdot 10^{-7}$	$8.5 \cdot 10^{-6}$	168	$5 \cdot 10^{-6}$	$4.2 \cdot 10^{-5}$
1000	3100	$1.2 \cdot 10^{-7}$	$4.2 \cdot 10^{-6}$			

**Table 1.** Accuracy of the penalty methods according to the penalty coefficient.

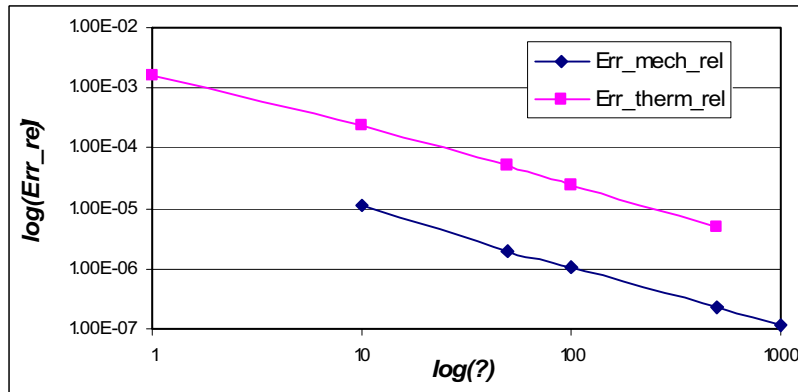
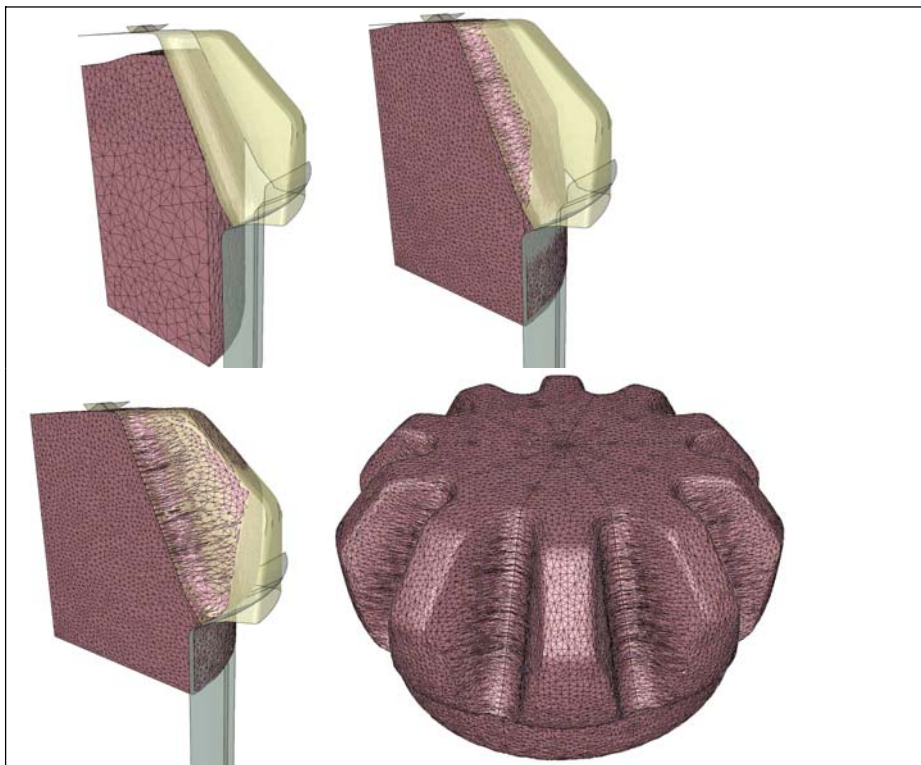


**Figure 10.** Error versus the value of the penalty coefficient in logarithmic scale.

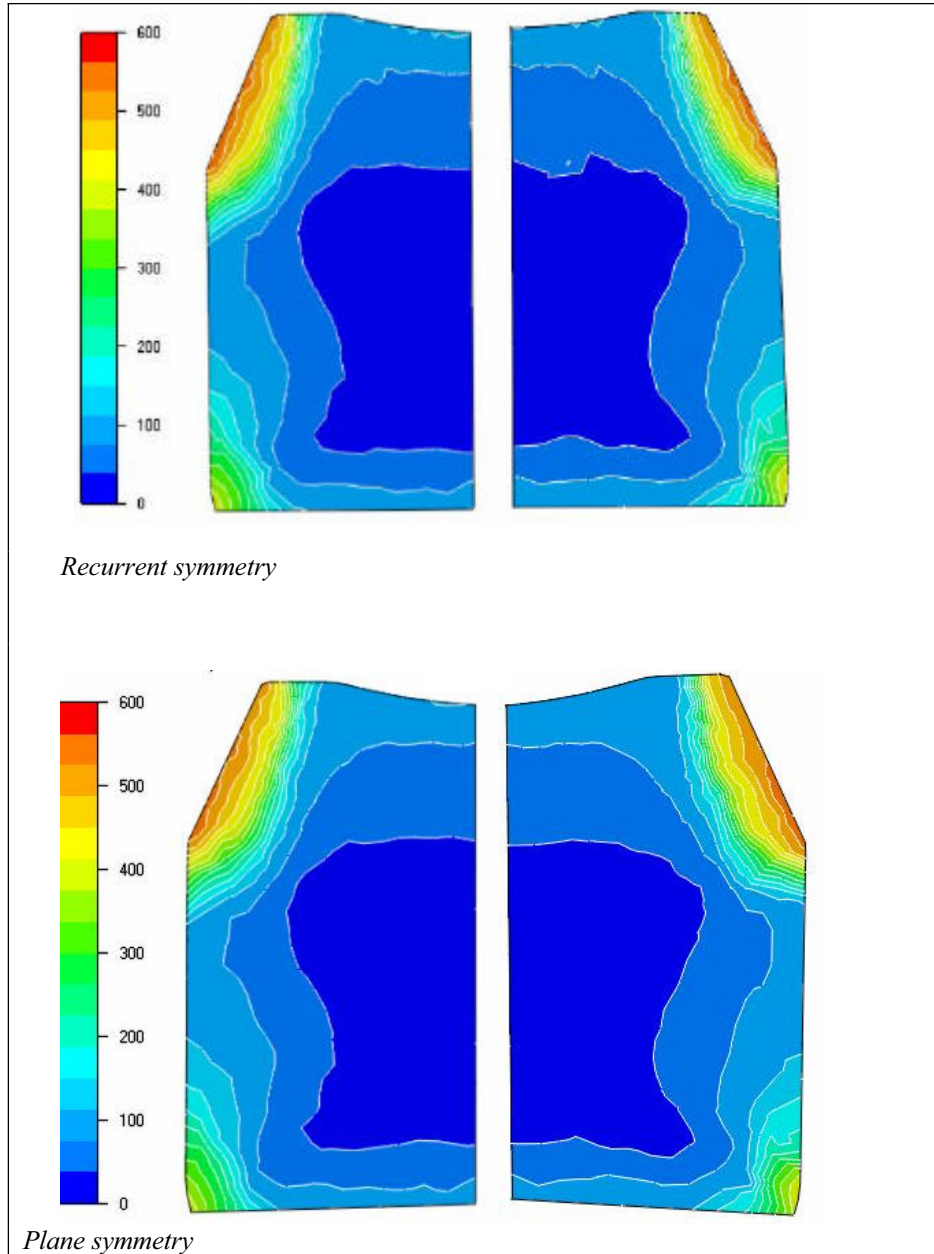
In this particular case with coincident meshes,  $\delta^k = 0$  so the  $\delta^k / \Delta t$  term does not appear in equations [50]. The errors are written in a similar way for the thermal problem.

Figure 10 shows that there is a linear dependency between the penalty coefficients and the mechanical and thermal errors, which is quite typical for a penalty method. On the other hand, table 1 shows that the CPU time (number of system resolutions) is increased by a factor of 2 when the errors are decreased by a factor of 10. Practically, penalty coefficients of 100 are used, both for mechanical and thermal problems, so providing accuracies that are consistent with the ones of the contact algorithm.

A second test consists in forging one tooth of an actual conical straight gear. The workpiece has a complex elasto-viscoplastic behaviour, and the tools have realistic geometries (see figure 11). This simulation is carried out both using plane symmetries and recurrent boundary conditions. In figure 11, the geometries are obtained with plane symmetries. The qualitative comparisons of figure 12 are made after few increments, just before the first remeshing, in order to make it possible to compare the values at exactly the same coordinates, and to avoid the noise caused by remeshing. The obtained results are almost identical with both approaches. For example, the values of the equivalent stress (see figure 12) and of the forging effort differ by less than  $10^{-4}$  in relative values.



**Figure 11.** Forging of a conical gear. Initial, intermediate and final configurations.



**Figure 12.** Equivalent stress on symmetry surfaces after 3 % of forging with plane and recurrent boundary conditions.

However, the CPU time is multiplied by a factor of 2 with recurrent conditions. This is due to the fact that the flow is less constrained while the coupling between the opposite sides of the domain is very severe. It results into a worsening of the conditioning of the linear system, and consequently into an increase of the computational time. This phenomenon is noticed in all numerical tests, independently on the complexity of the geometries or material behaviours. So, also taking into account that the computational complexity of the solver is proportional to  $N_{dof}^{3/2}$ , it is possible to evaluate the CPU time reduction provided by recurrent symmetries. For a helical gear with 10 teeth, the recurrent boundary conditions allow reducing the computational time by an estimated factor of 15.

#### **4.2. Industrial test: helical gear forging:**

The actual forging of a 16 teeth helical gear is considered (see figure 13), where the workpiece is free to rotate around its axis during the process. Consequently several teeth of the rigid matrix have to be considered for proper handling of the contact surface. The material is modelled by an elasto-viscoplastic constitutive equation.

Figures 14.a, 14.b and 14.c show that the velocity, temperature and deformation fields are almost identical on the master and the slave surfaces. So the velocity and temperature boundary conditions can be regarded as properly imposed, and the master/slave approach as quite accurate. At the end of the process, the gap between the corresponding symmetry faces provides an overall measure of the cumulated errors. It is less than  $10^{-4}$  in relative values (with respect to the mesh size) (see figure 14.d), which is consistent with the accuracy of the contact formulation. By duplicating and rotating the obtained final part, figure 15 shows that the corresponding surfaces match properly and that they have actually been subjected to the same deformations.

It is noticed that the workpiece rotates around the symmetry axis during forging, as it is the case in the actual process. In this case, the computational time reduction provided by this approach is estimated around 30.

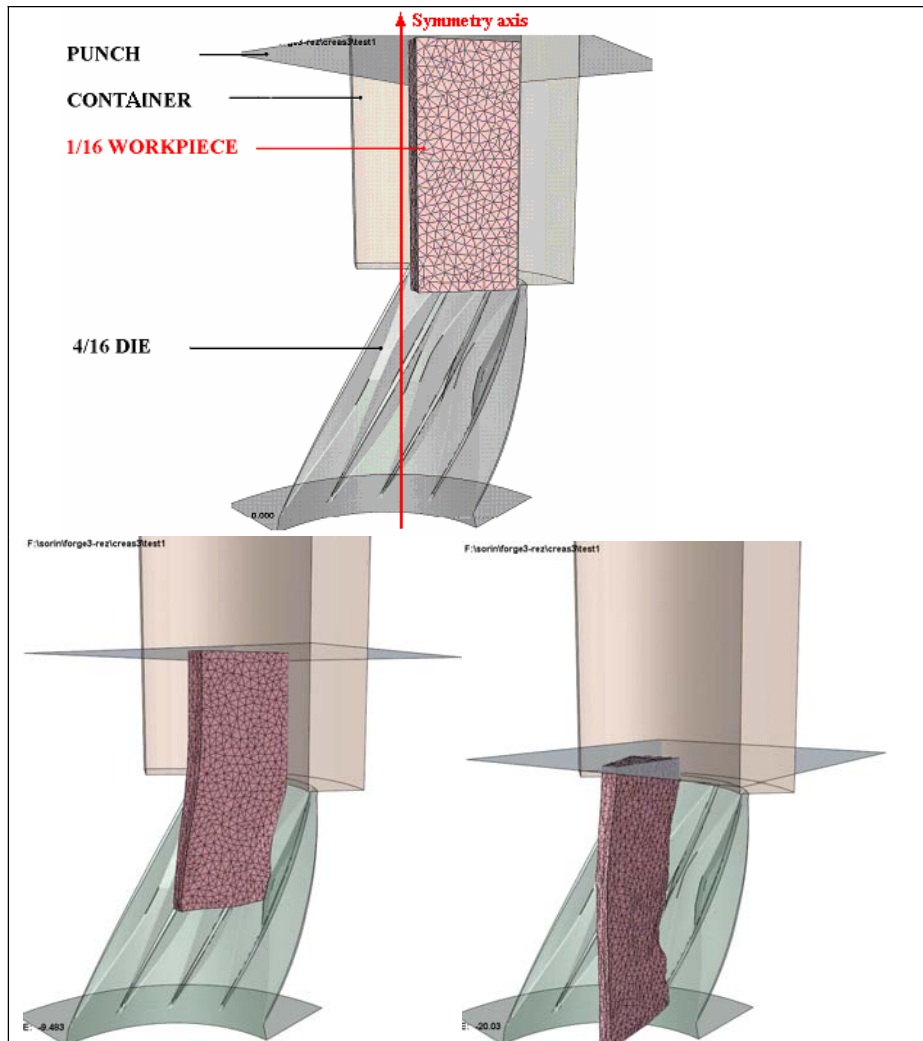


*Figure 13. Simulation of the actual forging of a helical gear.*

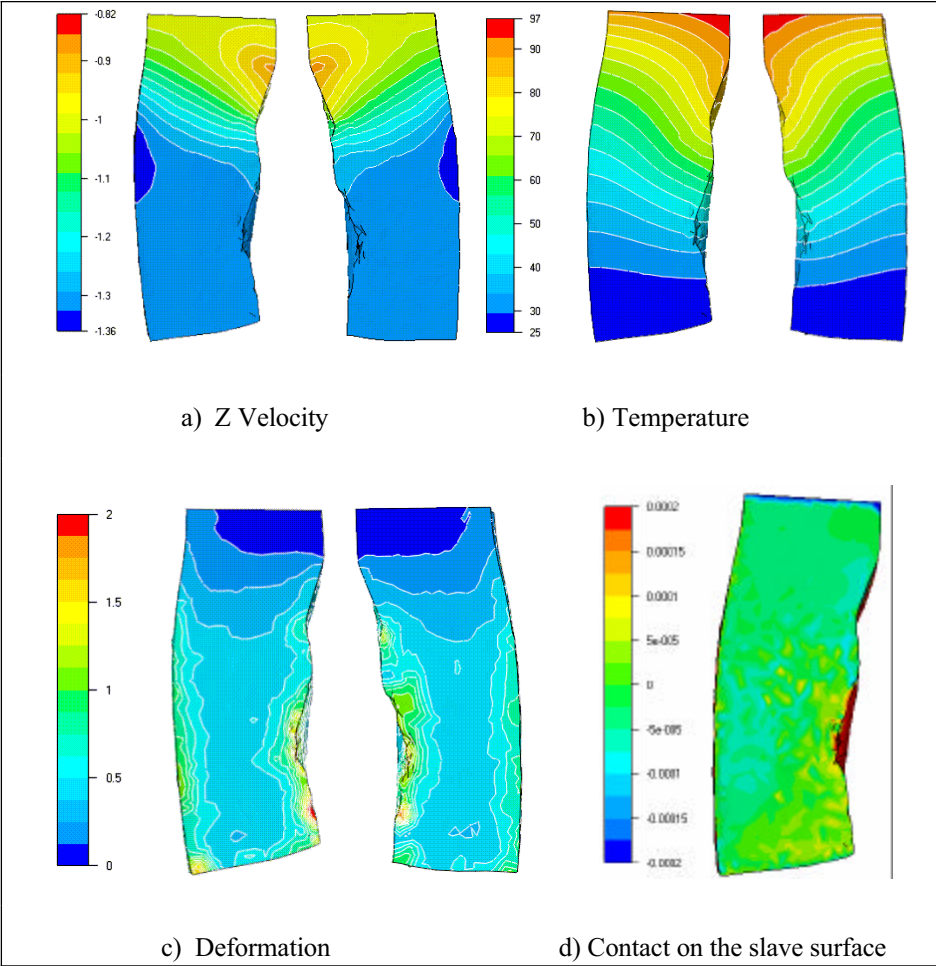
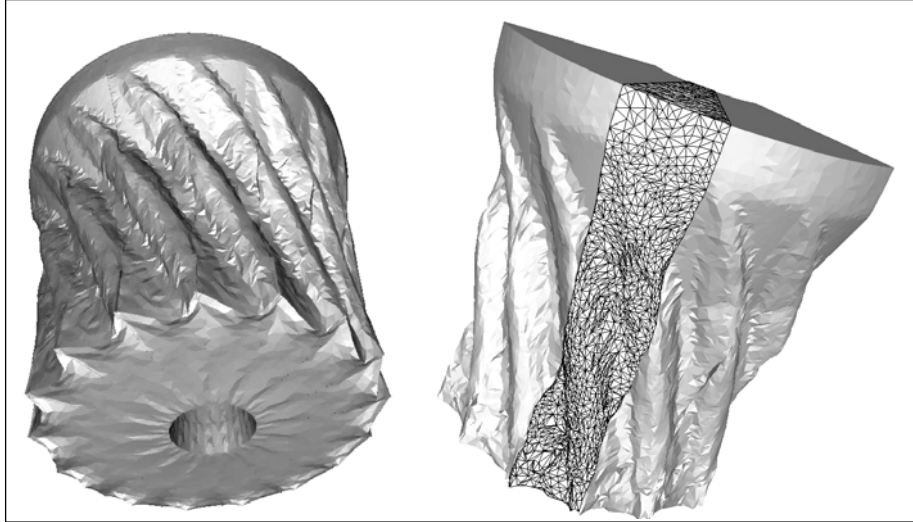


Figure 14. Isovalues on the master and slave surfaces.



**Figure 15.** Final configuration: fully reproduced and only with 5 teeth of the workpiece, while the simulation was carried out only on 1 tooth (mesh of left figure).

#### 4.3. Gear forging with deformable dies

In order to evaluate the accuracy and the robustness of the proposed approach with deformable tools, an academic gear-like forging process is proposed in figure 16. A viscoplastic constitutive law (with a linear behaviour,  $m_{part}=m_{tool}=1$ ) is used for the two bodies, workpiece and tool, in order to trigger complex velocity fields both on the symmetry surfaces and on the contact surfaces. However, the consistency  $K$  of the tool material is 10 times larger than the workpiece one:  $K_{part}=20MPa$ ,  $K_{tool}=200MPa$ .

As it can be seen in figure 16, “ghosts” surfaces are necessary from the beginning of the simulation, because the symmetry surfaces are not the same for the workpiece and for the tool. This particular case, which corresponds to a more friendly way to set up simulation data, can only be handled with the proposed method. In figure 17, it is very clear that the workpiece is in contact with the tool, both with its actual and ghost descriptions.

Figures 18 and 19 show that the recurrent symmetry conditions are accurately satisfied at the end of the calculations. Figure 18 shows that the contact conditions between the deformable bodies are properly imposed, even in the “ghost” zones. Both for the workpiece and for the deformable die, the gaps between the master and slave symmetry surfaces are very small, and can be regarded as negligible, as in previous example.

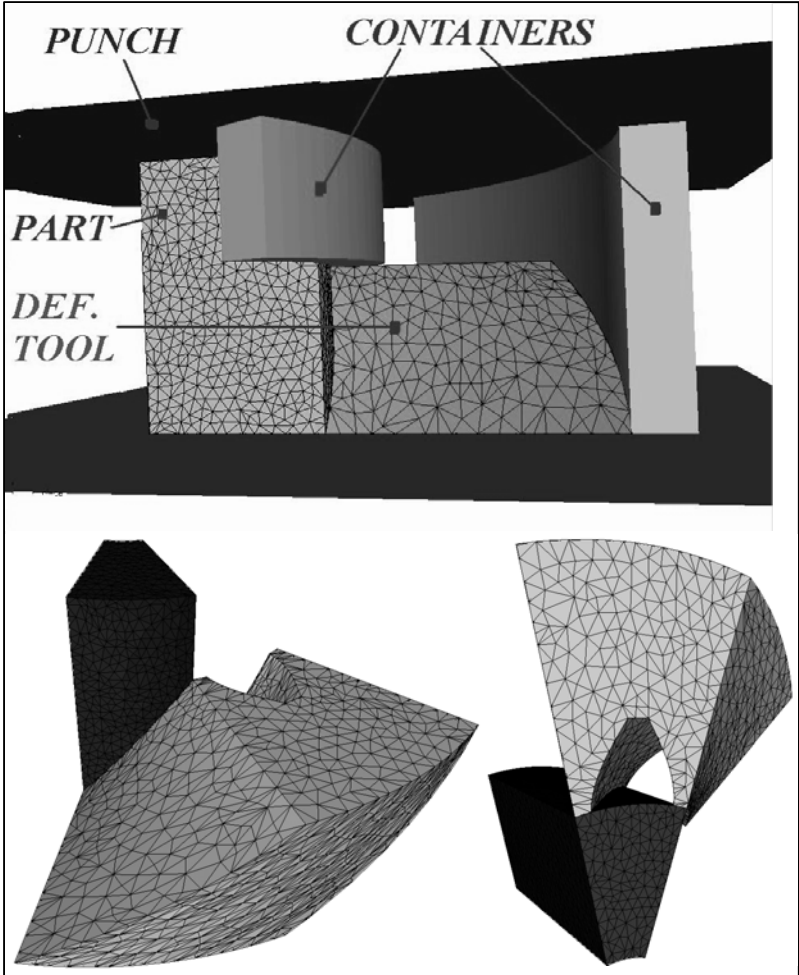


*Figure 16. Helical gear forging with deformable dies. Different views of the initial configuration and of the various tools, rigid (punch and container) and deformable.*

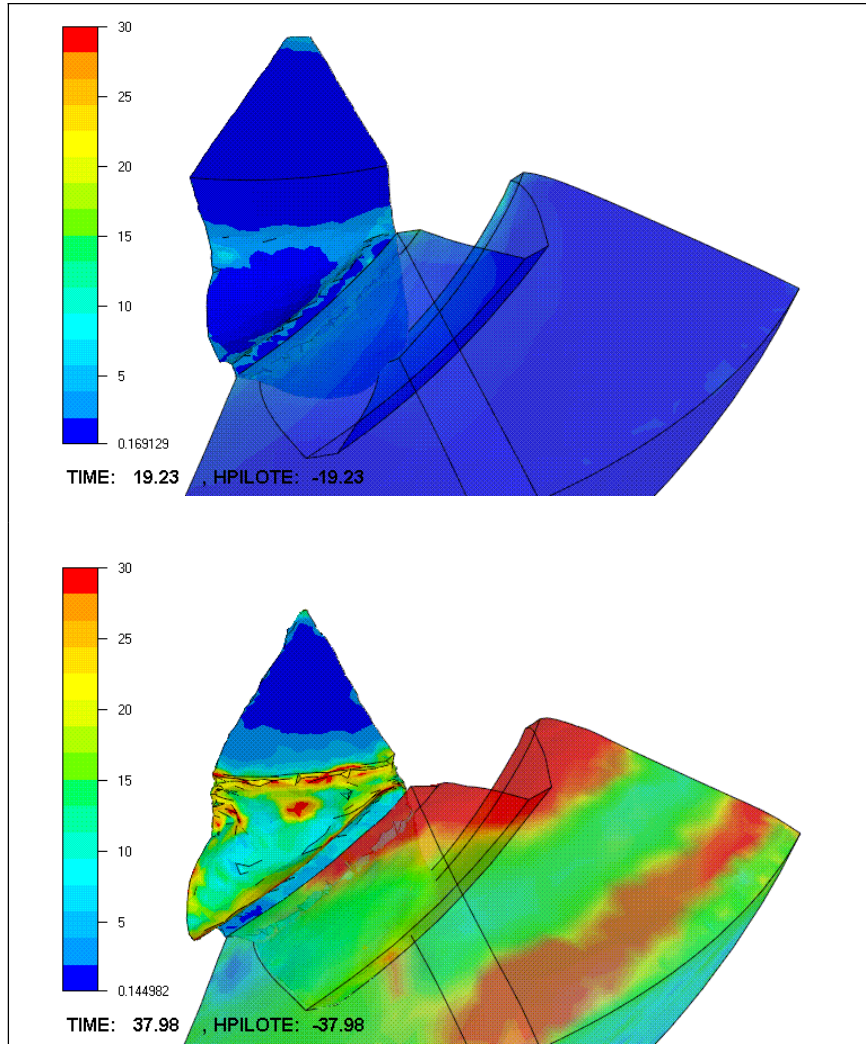


*Figure 17. Equivalent stress at two different stages of the process.*

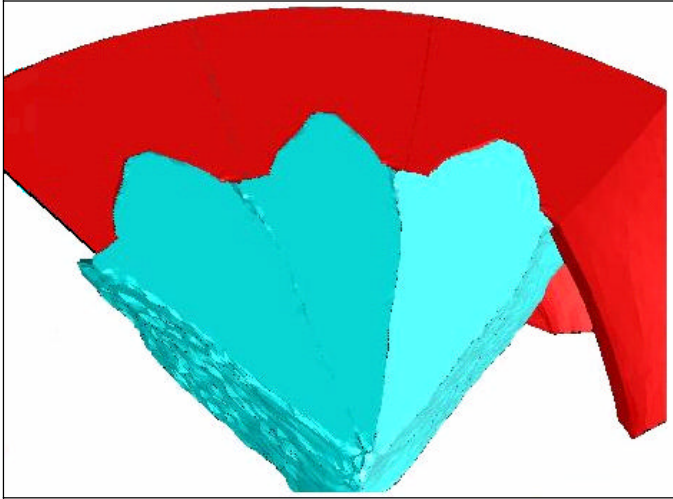


**Figure 18.** Forging of a helical gear with deformable dies: deformed tool and workpiece at the end of the process, after reconstruction of 3 teeth.

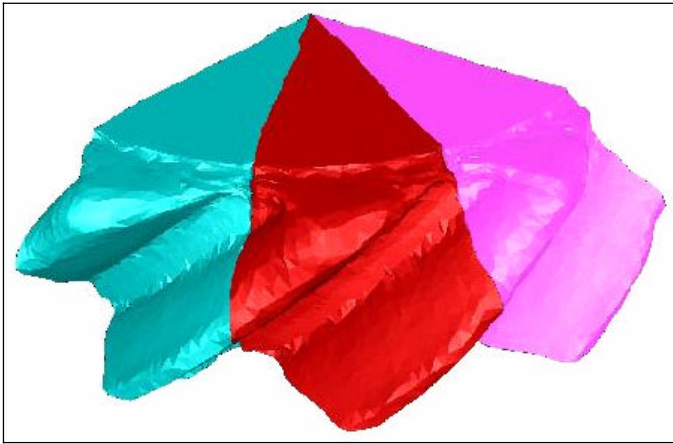


**Figure 19.** Forging of a helical gear with deformable dies: workpiece deformation after reconstruction of 3 teeth.

## 5. CONCLUSIONS

Recurrent boundary conditions are an efficient way to reduce the CPU time for helical gear simulation. The proposed implementation can be regarded like an extension of the bilateral contact algorithm between deformable surfaces. The utilised master / slave approach is both stable and accurate. It does not require coincident meshes or more complex formulations like Arbitrary Eulerian Lagrangian ones. The use of «ghost» surfaces makes it possible to extend it to multi-bodies problems, as encountered in the forging with deformable dies.

In some particular cases, this approach may suffer from some of the usual limitations of the master / slave method, if it happens that the symmetry surfaces exhibit very different mesh refinements. In these cases, it is possible that no recurrent boundary condition is imposed to some nodes of the master surface, which would provide locally wrong solutions. In order to avoid this, a more accurate contact formulations should be used, like the quasi-symmetric approach proposed in (Fourment et al. 04) or similar approaches.

## ACKNOWLEDGEMENTS

The authors gratefully acknowledge support from the French government and the companies involved in the Simulforge project managed by CETIM, and more particularly the Ascoforge company for providing the validation cases.

## REFERENCES

- Aliaga C., Massoni E., *3D numerical simulation of thermo-elasto-visco-plastic behaviour using stabilized mixed finite element formulation: application to heat treatment*, Proceedings of the Sixth International Conference on Numerical Methods in Industrial Forming Processes, Huetink, J.; Baaijens, F.P.T. (editors), A.A. Balkema, Rotterdam, Netherlands, pp 263-269, 1998
- Barboza J., Fourment L. and Chenot J.-L., *Contact algorithm for 3D multi-bodies problems: application to forming of multi-material parts and tool deflection*. In WCCM V - Fifth Congress on Computational Mechanics. 2002. Wien, Austria
- Bathe K.J. and Abbasi N.E., *On a new Segment to Segment Contact Algorithm*, in Computational Fluid and Solid mechanics, K.J Bathe, Editor. 2001, Elsevier Science
- Coupez T., *A mesh improvement method for 3d automatic remeshing*, Numerical Grid Generation in Computational Fluid Dynamics and Related Fields, pp 615-626, Weatherill, N.P. (editor), Pineridge Press, 1994
- Fourment L., Popa S. and Barboza J., *A Quasi-symmetric Contact Formulation For 3D Problems. Application To Prediction Of Tool Deformation In Forging*, The 8th Conference On Numerical Methods in Industrial Forming Processes, Columbus, Ohio, USA, June 2004

Huang G., *Gear Forging Simulation Using Cyclic Symmetry*, Proceedings of the Eighth International Conference on Numerical Methods in Industrial Forming Processes, Ghosh S., Castro J.M., Lee J.K. (editors), Springer-Verlag, New York, 1998

Park Y.B. and Yang D.Y., *Finite element analysis for precision cold forging of helical gear using recurrent boundary conditions*, Proc Instn Mech Engrs Vol 2/2 Part B, 7 October 1997

Pichelin E., Mocelin K., Fourment L. and Chenot J.-L., *An application of a master slave algorithm for solving 3D contact problems between deformable bodies in forming processes*, Revue Européenne des Eléments Finis, 10-8, 85, 2001

---

**PART 2. CONTACT BETWEEN DEFORMABLE  
BODIES  
QUASI-SYMMETRICAL APPROACH**



# A QUASI-SYMMETRIC CONTACT FORMULATION FOR LARGE 3D DEFORMATIONS SOLID MECHANICS

L. Fourment<sup>\*</sup>, S. Popa

*CEMEF, Ecole des Mines de Paris, B.P. 207, 06 904 Sophia Antipolis Cedex, France*

---

## Abstract

A quasi-symmetric formulation is proposed for contact between deformable bodies to avoid the shortcomings of standard master / slave approaches when the master body is more finely meshed than the slave body. It uses a double pass algorithm for symmetric contact detection and a projection of slave body contact pressures onto the master surface. This method applies either to integral or nodal contact formulations, the latter being used for applications. It is compared to the standard formulation for different numerical tests and on complex 3D forging applications.

*Keywords: Finite elements, Contact, Non matching meshes, Large deformations*

---

## 1. INTRODUCTION

This paper investigates a quasi-symmetric formulation for contact between deformable bodies, which has been developed to avoid the usual shortcomings of standard master / slave formulations without too many complications. It is well known that when the meshes of the contact interfaces do not match after finite element discretization, which is the most general case, the contact conditions cannot be handled symmetrically. The symmetric two-pass algorithms, where the contact conditions between body  $A$  and body  $B$  are super-imposed to the conditions between body  $B$  and  $A$ , produce over-constraint formulations with numerical locking of the contact interface [1-3]. In the standard master / slave approach, only the selected slave body is prevented from penetrating the master body. It so avoids locking. This approach is quite satisfactory when the bodies have meshes of consistent refinements on the contact interface. When they are matching, the formulation is perfectly symmetric. On the other hand, when the mesh of the master body is much finely refined than the mesh of the slave body, the formulation loses its symmetry, so the non-penetration condition is not properly imposed for the master surface. Consequently, it may occur that parts of this surface are numerically regarded as being free, which may allow significant and unacceptable penetrations. From a numerical point of view, the convergence rate of the finite element method is not only lower in this case, but the accuracy of the solution decreases when the number of the master nodes increases. This standard approach paradoxically provides worse and worse solutions when the master body is more finely refined.

---

<sup>\*</sup> Corresponding author. Tel. : +33 4 93 95 75 95 ; fax : +33 4 92 38 97 52  
E-mail address: lionel.fourment@ensmp.fr

This problem has motivated the development of several enhanced formulations, handling any of the three terms of the contact integral: the gap function, the integration surface and the Lagrange multiplier (i.e. the contact normal stress). All of these works, but the present one, have been developed in a facet-to-facet framework. In [4, 5], it is proposed to better compute the gap function by using a more accurate interpolation of the master displacement field on the slave surface. A global  $L^2$  projection provides this enhanced displacement field. It quite efficiently solves the discussed issues, but the computational cost of this approach is not negligible in 2D, and refrains from directly using it in 3D. In [2, 3, 6-8], it is preferred to better integrate the gap function by using a mortar surface, which is the merging of both master and slave discretized contact surfaces. In 2D, this construction is not too complex, and the method solves the contact issues [2, 6, 7]. In 3D, it requires building a new interface mesh that merges the two contacting meshes. It can be done locally, but it is a much more complex issue [3, 8].

Our motivation is to develop a formulation that reaches the same objectives, but also that can be more easily implemented into existing software, that can be utilized with a node-to-facet contact formulation, and that does not significantly increase the computational cost of the contact analysis. This approach is based on handling the third term of the contact integral, the Lagrange multiplier. After introducing the problem equations in section 2, the above mentioned contact formulations are presented in section 3. The proposed Quasi-Symmetric approach is then evaluated for several numerical contact tests proposed in other papers, before being utilized for complex 3D forging applications.

## 2. DEFORMABLE BODIES: CONTACT FORMULATIONS

Algorithms and equations are presented in the case of two deformable domains in contact, which are noted  $A$  and  $B$ . They can easily be extended to any number of parts. All the used  $l$  indexes refer to a node of the  $A$  master body, while all the  $k$  indexes refer to a node of  $B$  slave body. These conventions are used all along this paper.

### 2.1. Contact equations

When body  $B$  is in contact with body  $A$ , the contact equations are given by the Signorini conditions, on the potential contact surface  $\partial\Omega_B^{contact}$  :

$$\text{on } \partial\Omega_B^{contact}, \begin{cases} h_A \leq 0 \\ \sigma_n = \sigma_A n_A \cdot n_A = \sigma_B n_B \cdot n_B \leq 0 \\ \sigma_n h_A = 0 \end{cases} \quad (1)$$

where  $\sigma_A$  and  $\sigma_B$  respectively are the stress tensors on  $\Omega_A$  and  $\Omega_B$ ,  $n_A$  and  $n_B$  the outward normals to  $\Omega_A$  and  $\Omega_B$ .  $h_A$  is the gap function, which is negative for a point of  $\partial\Omega_B^{contact}$  if it does not penetrate body  $A$ , and else positive. For a velocity formulation,  $h_A$  is a function of  $v_A$  and is written as:

$$h_A(v_B) = (v_B - v_A) \cdot n_B - \frac{\delta^{BA}}{\Delta t} \quad (= h_A(v_B, v_A)) \quad (2)$$

where  $v_A$  and  $v_B$  respectively are the velocity fields on  $A$  and  $B$ ,  $\Delta t$  is a time step of the time discretization scheme,  $\delta^{BA}$  is the signed distance between  $B$  and  $A$  (see Figure 1), which is negative if a  $B$  point penetrates body  $A$ , and else positive. The symmetric contact equations

between  $A$  and  $B$  can similarly be written on  $\partial\Omega_A^{contact}$  :

$$\text{on } \partial\Omega_A^{contact}, \begin{cases} h_B \leq 0 \\ \sigma_n \leq 0 \\ \sigma_n h_B = 0 \end{cases} \quad (3)$$

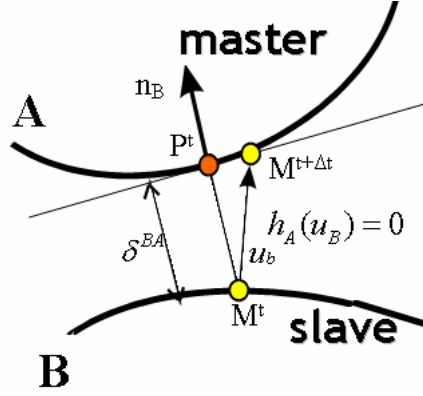


Figure 1: Contact between deformable bodies.

## 2.2. Problem statement

The mechanical problem equations are written for elastic and viscoplastic bodies, using a velocity formulation. They consist in finding the velocity fields  $v$  that minimize either the elasticity potential  $\Phi^{elast}(v)$  or the viscoplasticity potential  $\Phi^{visco}(v)$  under the constraint of being cinematically admissible (i.e. belonging to  $C^a$ ):

$$\Phi^{elast}(v) = \text{Min}_{u \in C^a} \Phi^{elast}(u) \quad (4)$$

$$\Phi^{visco}(v) = \text{Min}_{u \in C^a \cap C^i} \Phi^{visco}(u) \quad (5)$$

where  $C^a$  is the space of velocity fields that satisfy the contact constraints and  $C^i$  the space of incompressible fields.  $\Phi^{visco}(v)$  is given by:

$$\Phi^{visco}(v) = \int_{\Omega} \frac{K}{m+1} (\sqrt{3} \dot{\bar{\epsilon}})^{m+1} d\omega \quad (6)$$

where  $K$  is the material consistency,  $m$  the strain rate coefficient,  $\dot{\bar{\epsilon}} = \sqrt{\frac{2}{3} \dot{\epsilon} : \dot{\epsilon}}$  is the equivalent strain rate and  $\dot{\epsilon}$  is the strain rate tensor. The incompressibility constraint is handled by a mixed velocity / pressure  $(v, p)$  formulation and by solving a Max/Min problem:

$$\Lambda^{visco}(v, p) = \text{Max}_q \text{Min}_{u \in C^a} \Lambda^{visco}(u, q) \quad (7)$$

$$\text{where: } \Lambda^{visco}(v, p) = \Phi^{visco}(v) + \int_{\Omega} p \text{div}(v) d\omega \quad (8)$$

The contact constraint requires introducing contact Lagrange multipliers  $\lambda$  (i.e the normal contact stresses), writing new Lagrangians and solving new Max/Min problems:

$$\Lambda^{elasto}(v, \lambda) = \underset{0 \leq (-\mu)}{\text{Max}} \underset{u}{\text{Min}} \Lambda^{elasto}(u, \mu) \quad (9)$$

$$\text{where: } \Lambda^{elasto}(v, \lambda) = \Phi^{elasto}(v) + \Lambda(v, \lambda) \quad (10)$$

$$\Lambda^{visco}(v, p, \lambda) = \underset{0 \leq (-\mu)}{\text{Max}} \underset{q}{\text{Max}} \underset{u}{\text{Min}} \Lambda^{visco}(u, q, \mu) \quad (11)$$

$$\text{where: } \Lambda^{visco}(v, p, \lambda) = \Lambda^{visco}(v, p) + \Lambda(v, \lambda) \quad (12)$$

The contact Lagrangian introduced in (10) and (12) is given by:

$$\Lambda(v, \lambda) = \Lambda_B = \int_{\partial\Omega_B^{contact}} h_A(v_B) \lambda^B ds_B \quad (13)$$

$$\text{or else : } \Lambda(v, \lambda) = \Lambda_A = \int_{\partial\Omega_A^{contact}} h_B(v_A) \lambda^A ds_A \quad (14)$$

where  $\lambda^A$  and  $\lambda^B$  respectively are the contact Lagrange multipliers on bodies  $A$  and  $B$ . At the continuous level, both Lagrangians are equivalent, so:

$$\Lambda = \Lambda_A = \Lambda_B \quad (15)$$

### 2.3. Finite element discretization

For space discretization, an unstructured mesh of tetrahedra is used with a P1+/P1 velocity/pressure interpolation.

$$x(\zeta) = \sum_{n=1}^{Nbn} X_n N_n(\zeta) \quad (16)$$

$$v(\zeta) = \sum_{n=1}^{Nbn} V_n N_n(\zeta) + \sum_{e=1}^{Nelt} V_e \Phi_e(\zeta) = v_l + v_b \quad (17)$$

where  $Nbn$  is the number of nodes of the mesh,  $Nelt$  is the number of elements,  $\zeta$  are the local coordinates of  $X$ ,  $N_n$  the linear interpolation function at node  $n$  and  $\Phi_e$  the linear “bubble” interpolation function of element  $e$  ( $\Phi_e$  vanishes on the surface).

This work has been carried out in the frame of the FORGE3® software, where a nodal (node-to-facet) contact formulation is utilized. Therefore, the discretized form of the equations are presented in this specific case.

### 3. CONTACT FORMULATIONS

#### 3.1. Master / slave

The master/slave method consists in computing a single Lagrangian,  $\Lambda_B$ :

$$\Lambda^{M/S} = \Lambda_B = \int_{\partial\Omega_B^{\text{contact}}} h_A(v_B) \lambda^B ds_B \quad (18)$$

For the nodal (node-to-facet) contact formulation, the contact conditions (1) are written for any node of the potential contact surface,  $\partial\Omega_B^{\text{contact}}$ , and the Lagrangian (13) yields:

$$\Lambda^{M/S} = \sum_{k \in \partial\Omega_B^{\text{contact}}} h_A(V_k) \lambda_k^B S_k \quad (19)$$

$$\text{where: } \forall k \in \partial\Omega_B^{\text{contact}}, \quad h_A(V_k) = (V_k - V_{\pi^A(k)}) \cdot n_B^k - \frac{\delta_k^{BA}}{\Delta t} \quad (20)$$

$\pi^A(k)$  is the orthogonal projection of node  $k$  on the master body  $A$ .  $S_k$  is a surface associated to node  $k$  that is calculated by:

$$S_k = \int_{\partial\Omega_B} N_k^B ds \quad (21)$$

The velocity of  $\pi^A(k)$  is obtained by using the finite element interpolation on the master facet  $f_A^k$  that contains the projection  $\pi^A(k)$ :

$$V_{\pi^A(k)} = \sum_{l \in f_A^k} N_l^A(\zeta_A^k) \cdot V_l \quad (22)$$

where  $\zeta_A^k$  are the local coordinates on  $f_A^k$  of the projection  $\pi^A(k)$ .

This method has several advantages and some shortcomings. It is easy to implement and it is not expensive in terms of CPU time for 3D formulations. However, due to a bad treatment of the contact interface, its convergence rate is not always satisfactory and can be decreased with respect to the usual rate of the finite element method without contact conditions. Moreover, when the master body has a finer mesh than the slave one, some nodes of the contact interface may not have contact boundary conditions, as shown in Figure 2. So, rather than finding a better solution with a finer mesh of the master body, the contrary is obtained.

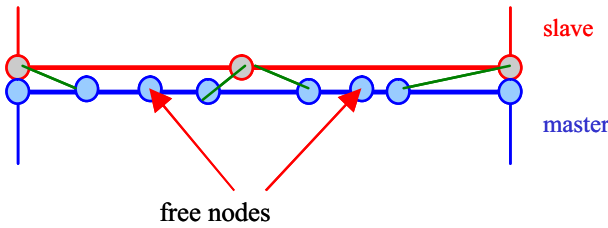
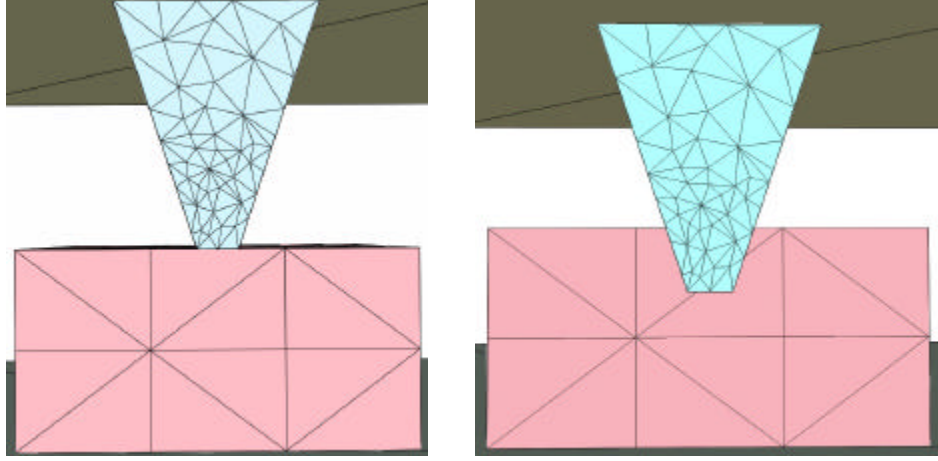


Figure 2: Finer mesh for the master body. Some nodes of the contact surface have no contact boundary condition.

An extreme case is presented in Figure 3. The indented slave body is too coarse to detect the contact event, because there is not any slave node  $k$  in contact with the indenter master body. There is not any contact contribution, so the bodies penetrate each other without detecting their respective presences. This extreme configuration is a benchmark to evaluate the robustness of the contact algorithm.



*Figure 3: Indentation of a coarse part (slave) with a fine indenter (master). Initial and final configurations. No contact is detected between the two bodies*

### 3.2. Two pass

An easy way to avoid such shortcomings is to use a two-pass algorithm, by sequentially or simultaneously imposing contact conditions between  $B$  and  $A$ , using the  $\Lambda_B$  Lagrangian, and between  $A$  and  $B$ , using the  $\Lambda_A$  Lagrangian. It so provides a perfectly symmetric formulation, as presented for instance in [9], where the contact equations are integrated on the two body interfaces using the following Lagrangian:

$$\Lambda^{SYM} = \frac{1}{2}(\Lambda_B + \Lambda_A) = \frac{1}{2} \left( \int_{\partial\Omega_B^{contact}} h_A(v_B) \lambda^B ds_B + \int_{\partial\Omega_A^{contact}} h_B(v_A) \lambda^A ds_A \right) \quad (23)$$

However, with non matching meshes, this method provides an over-constrained problem [1, 2, 8] as shown in the following example. In Figure 4a, the meshes match so the symmetric approach is identical to the master / slave one. There are  $2n+2$  contact conditions, which are identical two by two, so they reduce to actually  $n+1$  distinct conditions. In this 2D example, there are  $2n+2$  degrees of freedom, so the surface does not lock. However, in Figure 4b the meshes do not match, so the number of contact equations is not reduced. There are  $2n$  distinct equations. If they are all satisfied, there are only 4 remaining degrees of freedom for the deformation of the interface (instead of  $n+1$  in the previous case). Therefore, this deformation can only be linear: the contact surface is artificially stiff. In other words, the number of degrees of freedom for the interface deformation does not depend on the number of interface nodes. It corresponds to a finite element discretization with only 2 nodes. On the other hand, it should be noticed that when the master and slave surfaces have a very different level of discretization, for instance as in Figure 3, the added unnecessary constraints do not introduce important locking. In such cases, the two-pass method provides a better solution than the master /slave one.

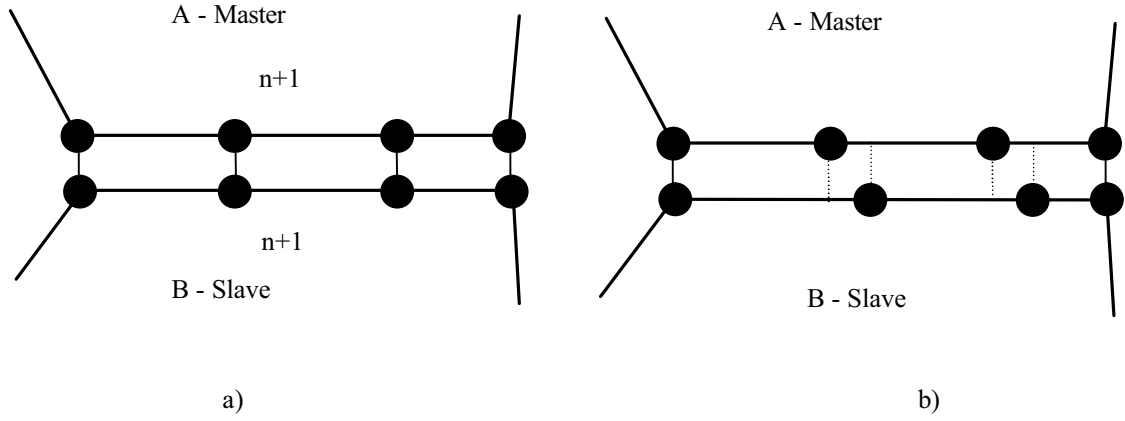


Figure 4: Over constraint problem with the symmetrical approach. In b), the nodes are slightly moved by a small displacement.

Therefore, almost all the methods that have been developed to circumvent these shortcomings have been carried out in the master / slave paradigm.

### 3.3. Integral joint

In [4], a different method is proposed. It consists in integrating the contact equation on the slave body and using a global  $L^2$  projection to interpolate the velocity field on the master body. As previously, the contact Lagrangian (13) has to be integrated, but it now writes:

$$\Lambda^{IJ} = \int_{\partial\Omega_B^{\text{contact}}} \tilde{h}_A(v_B) \lambda^B ds \quad (24)$$

$$\text{where: } \tilde{h}_A(v_B) = (v_B - \tilde{v}_A) \cdot n_B - \frac{\delta^{BA}}{\Delta t} \quad (25)$$

$$\tilde{v}_A \text{ is interpolated on the } \partial\Omega_B \text{ surface by: } \tilde{v}_A = \sum_{k \in \partial\Omega_B^{\text{contact}}} \tilde{v}_A^k N_k^B \quad (26)$$

In order that  $\tilde{v}_A$  be a global  $L^2$  projection of  $v_A$  onto  $\partial\Omega_B$ ,  $(\tilde{v}_A^k)_k$  minimizes the following least square functional:

$$\Pi^{IJ} \left( (\tilde{v}_A^k)_k \right) = \int_{\partial\Omega_B^{\text{contact}}} (v_A - \tilde{v}_A)^2 ds \quad (27)$$

This interpolation ensures boundary conditions for all master nodes, so preventing the master body to penetrate the slave one, and provides a better convergence rate to the finite element method [4, 10]. On the other hand, the resolution of (27) and the increase of the problem bandwidth, which results from (25) and (26), quite significantly increase the problem complexity and the resulting computational time.

### 3.4. Mortar method

The Mortar method offers another efficient way to answer the contact issues. It can be regarded as an improved way to compute the  $\Lambda_B$  integral (13), using the best possible integration surface from the finite element standpoint. An improved discretization of  $\partial\Omega_B^{contact}$ ,  $\bar{\Gamma}_C$  is built, which results from the merge of  $\partial\Omega_B^{contact}$  and the projection of  $\partial\Omega_A^{contact}$  onto  $\partial\Omega_B$ . It so contains both the nodes of  $\partial\Omega_B^{contact}$  and the projections of the nodes of  $\partial\Omega_A^{contact}$  onto  $\partial\Omega_B$  (see Figure 5):

$$\forall c \in \bar{\Gamma}_c, \begin{cases} \exists k \in \partial\Omega_B^{contact}, c = k \\ \text{or} \\ \exists l \in \partial\Omega_A^{contact}, c = \pi^B(l) \end{cases} \quad (28)$$

$$\text{and then: } \Lambda^{mortar} = \int_{\bar{\Gamma}_C} \bar{h}_A(v_B) \lambda^B ds_{\bar{\Gamma}_C} \quad (29)$$

Integrating  $\Lambda^{mortar}$  on  $\bar{\Gamma}_C$  allows an accurate calculation of  $\bar{h}_A(v_B)$  on both surfaces,  $\partial\Omega_B^{contact}$  and  $\partial\Omega_A^{contact}$ . In fact, any node of  $\bar{\Gamma}_C$  either belongs to  $\partial\Omega_B^{contact}$ , and so  $h_A(v_B)$  is easily calculated, or is the projection of a node of  $\partial\Omega_A^{contact}$  onto  $\partial\Omega_B^{contact}$ , and so  $h_B(v_A)$  is known. Therefore,  $\bar{h}_A(v_B)$  can be interpolated using the nodal interpolation functions of  $\bar{\Gamma}_C$ . On the other hand, as  $\bar{\Gamma}_C$  contains  $\partial\Omega_B^{contact}$ ,  $\lambda^B$  is naturally interpolated using the  $\partial\Omega_B$  interpolation functions.

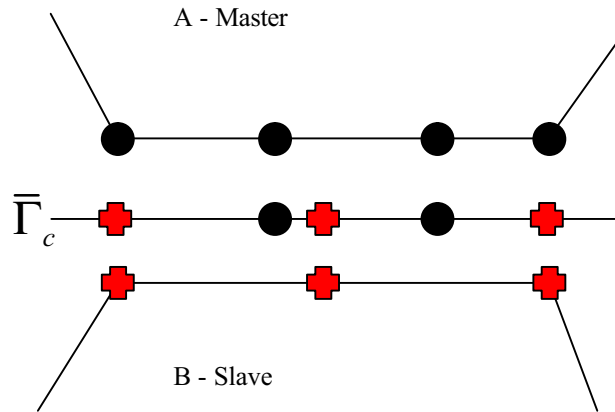


Figure 5: Mortar surface  $\bar{\Gamma}_C$  for an accurate integration of the gap function  $\bar{h}_A(v_B)$ .

All implementations have been carried out in the frame of a segment-to-segment (or facet-to-facet in 3D) frame. The Mortar method provides very nice results in 2D [2, 6, 7]. In 3D, the construction of  $\bar{\Gamma}_C$  is much more complex, but recent papers [3, 8] show that it is quite feasible.

### 3.5. Quasi-Symmetric formulation

On the one hand, the Quasi-Symmetric formulation can be regarded as a more rigorous way to utilize the two-pass algorithm. On the other hand, it can be considered as a simplified way to approach both the Mortar and the Integral Joint methods by focusing the analysis on the Lagrange multipliers rather than on the gap function or on the integration surface. Being based on the projection of the Lagrange multiplier  $\lambda^B$  on  $\partial\Omega_A$ , it so provides a counterpart to the projection of  $v_A$  on  $\partial\Omega_B$  in the Integral Joint formulation. Finally, contrary to the Mortar method, it is not restricted to integral (facet-to-facet) contact formulations and can easily be extended to nodal (node-to-facet) contact formulations.

In the two-pass symmetric formulation presented in section 3.2., the locking phenomenon actually arises from the utilization of Lagrange multipliers,  $\lambda$  on both contact surfaces,  $\partial\Omega_A$  and  $\partial\Omega_B$ . This locking can be avoided if the Lagrange multipliers are defined on a single body, the slave one,  $\partial\Omega_B$ . This can be done by using the projection of  $\lambda^B$  onto  $\partial\Omega_A$ , instead of  $\lambda^A$  in equation (23). The Quasi-Symmetric method is then summarized in the following equations:

$$\Lambda_A \approx \bar{\Lambda}_A = \int_{\partial\Omega_A^{\text{contact}}} h_B(v_A) \bar{\lambda}^B ds_A \quad (30)$$

$$\text{and then: } \Lambda^{QS} = \frac{1}{2}(\Lambda_B + \bar{\Lambda}_A) = \frac{1}{2} \left( \int_{\partial\Omega_B^{\text{contact}}} h_A(v_B) \lambda^B ds_B + \int_{\partial\Omega_A^{\text{contact}}} h_B(v_A) \bar{\lambda}^B ds_A \right) \quad (31)$$

where  $\bar{\lambda}^B$  is the projection of the normal stress multiplier  $\lambda^B$  onto  $\partial\Omega_A$ . It can be noticed that equation (31) is very similar to equation (23). The replacement of  $\lambda^A$  by  $\bar{\lambda}^B$  in (30) brings the necessary and sufficient enhancement that allows eliminating the unnecessary contact conditions that result into locking.

With an integral, facet-to-facet, contact formulation, the finite element discretization of equation (30) is straightforward. In fact, it is only necessary to compute  $\bar{\lambda}^B$ , which is a continuous field like  $\lambda^B$ . Both are interpolated with the velocity finite element functions as:

$$\lambda^B(\zeta) = \sum_{k \in \partial\Omega_B^{\text{contact}}} \lambda_k^B N_k^B(\zeta) \quad \text{and} \quad \bar{\lambda}^B(\zeta) = \sum_{l \in \partial\Omega_A^{\text{contact}}} \bar{\lambda}_l^B N_l^A(\zeta) \quad (32)$$

where  $N_k^B$  and  $N_l^A$  are the linear interpolation functions. Here, it is not necessary to use an enhanced  $L^2$  projection operator as in the integral joint method. A simple orthogonal projection is sufficient. The interpolation parameter  $\bar{\lambda}_l^B$  of  $\bar{\lambda}^B$  is the value of  $\lambda^B$  at point  $\pi^B(l)$ , the projection of node  $l$  onto  $\partial\Omega_B$ . It is so given by:

$$\forall l \in \partial\Omega_A^{\text{contact}}, \quad \bar{\lambda}_l^B = \lambda^B(\pi^B(l)) = \sum_{k \in f_B^l} \lambda_k^B N_k^B(\zeta_B^l) \quad (33)$$

where  $f_B^l$  denotes the facet of  $\partial\Omega_B$  that contains the orthogonal projection  $\pi^B(l)$ , and  $\zeta_B^l$  are the coordinates of this projection. So:

$$\bar{\lambda}^B(\zeta) = \sum_{l \in \partial\Omega_A^{contact}} N_l^A(\zeta) \sum_{k' \in f_B^l} \lambda_{k'}^B N_{k'}^B(\zeta^l) \quad (34)$$

For the utilized nodal (node-to-facet) contact formulation, in a rigorous way, the construction of  $\bar{\lambda}^B$  is not as straightforward, because  $\lambda^B$  and  $\bar{\lambda}^B$  are not continuous fields. First, equation (31) is written as:

$$\Lambda^{QS} = \frac{1}{2} \sum_{k \in \partial\Omega_B^{contact}} h_A(V_k) \lambda_k^B S_k^B + \frac{1}{2} \sum_{l \in \partial\Omega_A^{contact}} h_B(V_l) \bar{\lambda}_l^B S_l^A \quad (35)$$

As in equation (19), it is preferred to weight the contribution of any node  $k$  or  $l$  with the surface  $S_k$  or  $S_l$  (see equation (21)), in order to better control the material flow through the obstacle. The definition of the “gap” function (20) is written again for any node belonging to  $\partial\Omega_B$  or  $\partial\Omega_A$ :

$$\forall k \in \partial\Omega_A^{contact}, \quad h_A(V_k) = \sum_{i=1}^3 \left[ \left( V_{ik} - \sum_{l \in f_A^k} N_l^A(\zeta_A^k) \cdot V_{il} \right) \cdot n_{ik}^B \right] - \frac{\delta_k^{BA}}{\Delta t} \quad (36)$$

$$\forall l \in \partial\Omega_B^{contact}, \quad h_B(V_l) = \sum_{i=1}^3 \left[ \left( V_{il} - \sum_{k \in f_B^l} N_k^B(\zeta_B^l) \cdot V_{ik} \right) \cdot n_{il}^A \right] - \frac{\delta_l^{AB}}{\Delta t} \quad (37)$$

where  $i$  denotes the directions of space. The main issue is now to define  $\bar{\lambda}^B$  on  $\partial\Omega_A^{contact}$ , and more precisely for any nodes of  $\partial\Omega_A^{contact}$ . First, following what has been done with the integral contact formulation, at any node  $l$  of  $\partial\Omega_A^{contact}$ , the value of  $\bar{\lambda}^B$  is approximated by the value of  $\lambda^B$  at  $\pi^B(l)$ , the projection of node  $l$  onto  $\partial\Omega_B$ :

$$\bar{\lambda}_l^B = \bar{\lambda}^B(l) \approx \lambda_{\pi^B(l)}^B \quad (38)$$

However, with the nodal contact formulation,  $\lambda^B$  is not a continuous field; it is only defined for the nodes of  $\partial\Omega_B^{contact}$ . Rigorously, we could use the dual mesh of the contact surface, with a piecewise interpolation of  $\lambda^B$ , but we prefer using a more continuous interpolation and carry on as with the integral contact formulation. The second approximation then consists into extrapolating  $\lambda^B$  at any point of  $\partial\Omega_B^{contact}$ , assuming that  $\lambda^B$  is interpolated with the velocity functions:

$$\bar{\lambda}_l^B = \lambda_{\pi^B(l)}^B = \sum_{k' \in f_B^l} \lambda_{k'}^B N_{k'}^B(\zeta_B^l) \quad (39)$$

Finally, equation (35) yields:

$$\Lambda^{QS} = \frac{1}{2} \left( \sum_{k \in \partial\Omega_B^{contact}} \lambda_k^B S_k^B h_A(V_k) + \sum_{l \in \partial\Omega_A^{contact}} S_l^A h_B(V_l) \sum_{k' \in f_B^l} \lambda_{k'}^B N_{k'}^B(\zeta_B^l) \right) \quad (40)$$

Equation (40) clearly shows that the Quasi-Symmetric formulation is actually a master/slave one, because the Lagrange multipliers are defined only on  $\partial\Omega_B$ . In this sense, it is similar to

its standard master/slave counterpart (19). However, the second member of (40) is significantly different from (19). It is an average of non-penetration conditions for nodes of both  $\partial\Omega_B^{contact}$  and  $\partial\Omega_A^{contact}$ . This formulation is Quasi-Symmetric in the sense that the two bodies contribute in a balanced way to this condition. If the discretization of  $\partial\Omega_A^{contact}$  is finer than the one of  $\partial\Omega_B^{contact}$ , then all nodes of  $\partial\Omega_A^{contact}$  will be taken into account, which was not the case with the standard master/slave formulation. Even in the extreme example of Figure 3, the Lagrange multipliers of  $\partial\Omega_B^{contact}$  have a non-zero contribution, so making it possible to handle the contact event. The Quasi-Symmetric unilateral contact condition is now derived from equation (40), and written for any node of  $\partial\Omega_B^{contact}$  as:

$$\forall k \in \partial\Omega_B^{contact}, \quad h_A(V_k) + \sum_{\substack{l \in \partial\Omega_A \\ s.t. k \in f_B^l}} \frac{S_l^A}{S_k^B} N_k^B(\zeta_B^l) h_B(V_l) \leq 0 \quad (41)$$

For the applications, a penalty formulation is utilized to enforce the contact conditions. Therefore, the equations (10) and (12) in the elastic and viscoplastic cases, are replaced by the following functional and Lagrangian:

$$\Phi_\rho^{elasto}(v) = \Phi^{elasto}(v) + \rho \Phi^{contact}(v) \quad (42)$$

$$\Lambda_\rho^{visco}(v, p) = \Lambda^{visco}(v, p) + \rho \Phi^{contact}(v) \quad (43)$$

where  $\rho$  is a large penalty parameter and  $\Phi^{contact}(v)$  is given by:

$$\Phi_{QS}^{contact}(v) = \frac{1}{2} \sum_{k \in \partial\Omega_B^{contact}} S_k^B \left[ h_A(V_k) + \sum_{\substack{l \in \partial\Omega_A \\ s.t. k \in f_B^l}} \frac{S_l^A}{S_k^B} N_k^B(\zeta_B^l) h_B(V_l) \right]^{+2} \quad (44)$$

where  $[x]^+ = \frac{x + |x|}{2}$  is the positive part function.

## 4. VALIDATIONS

In order to evaluate the efficiency of the Quasi-Symmetrical formulation, several numerical tests are considered. Some are classical ones that are extracted from literature, like the contact patch test and the constant pressure test, while others are new or derived from other papers.

### 4.1. Convergence rate

This upsetting test aims at numerically estimating the convergence rate of the Quasi-Symmetrical formulation. Two identical bars are flattened between two rigid dies under plane deformation conditions (see Figure 6) with a prescribed uniform displacement. They have a linear elastic behavior, with a Poisson coefficient  $\nu = 0.3$  and a Young modulus  $E = 3 \cdot 10^4$  MPa (for the lower master body) and  $E = 1.3 \cdot 10^4$  MPa (for the upper slave body). The contact with the rigid tools and between the deformable bodies is perfectly sticking.

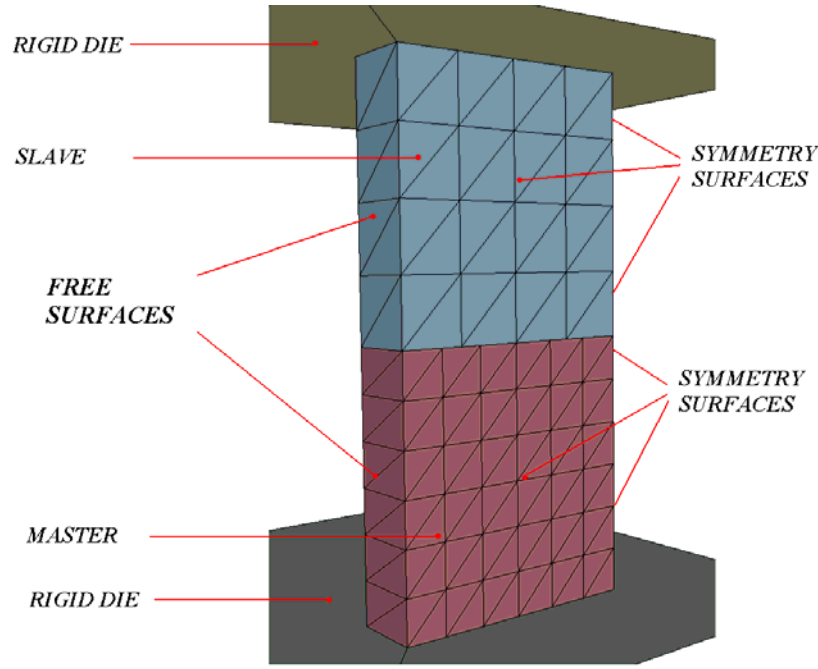


Figure 6: Boundary conditions and meshes (case n°3) for the convergence test.

The approximated problem solution is calculated on a reference mesh, which is four times finer than the finest studied mesh. The relative error,  $E_r$ , is then defined by the difference between the calculated forging force  $F$ , and the value calculated on the reference mesh,  $F_{ref}$  :

$$E_r = \frac{F - F_{ref}}{F_{ref}} \quad (45)$$

Mesh size		Reference	Case n°1	Case n°2	Case n°3	Case n°4	Case n°5
Matching		1	4	8	16	32	64
Non matching	Master	1.33	5.3	10.6	21.3	42.6	x
	Slave	2	8	16	32	64	x

Table 1: Sizes of the different studied meshes in the convergence test both for matching (master is similar to slave) and non matching set-ups.

The studied set of embedded meshes is presented in Table 1. They are produced from the coarsest mesh (which is denoted as case n°5 in the set of matching meshes and as case n°4 in the set of non matching ones, by a uniform refinement procedure of a factor 2 in each space direction (see Figure 7 and Figure 8). When the meshes of the master and slave bodies are similar (see Figure 7), the discrete contact surfaces are matching. Both formulations, Standard and Quasi-Symmetric, provide the same results, and the calculated convergence rate is the one of the finite element method. For the non matchings embedded meshes (see Figure 8), the master body is more finely meshed than the slave body with a ratio  $\frac{3}{2}$ .

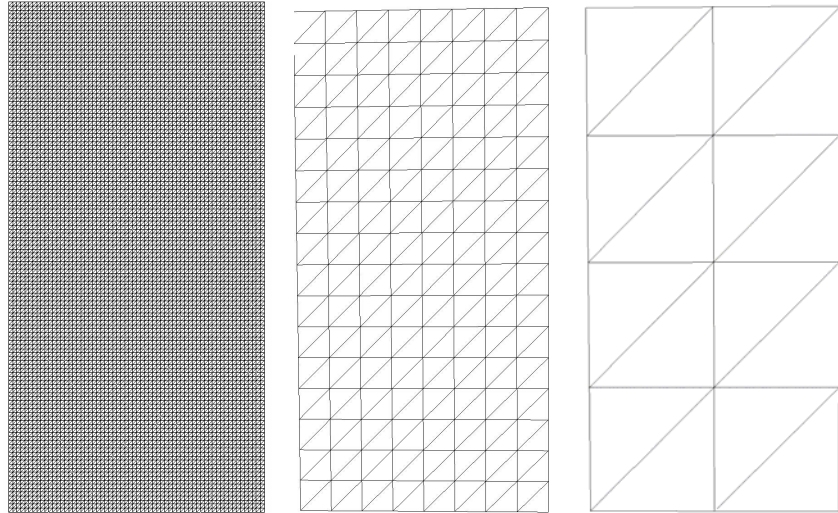


Figure 7: Matching meshes for the convergence test: cases  $n^{\circ}1$ ,  $n^{\circ}3$ , and  $n^{\circ}5$

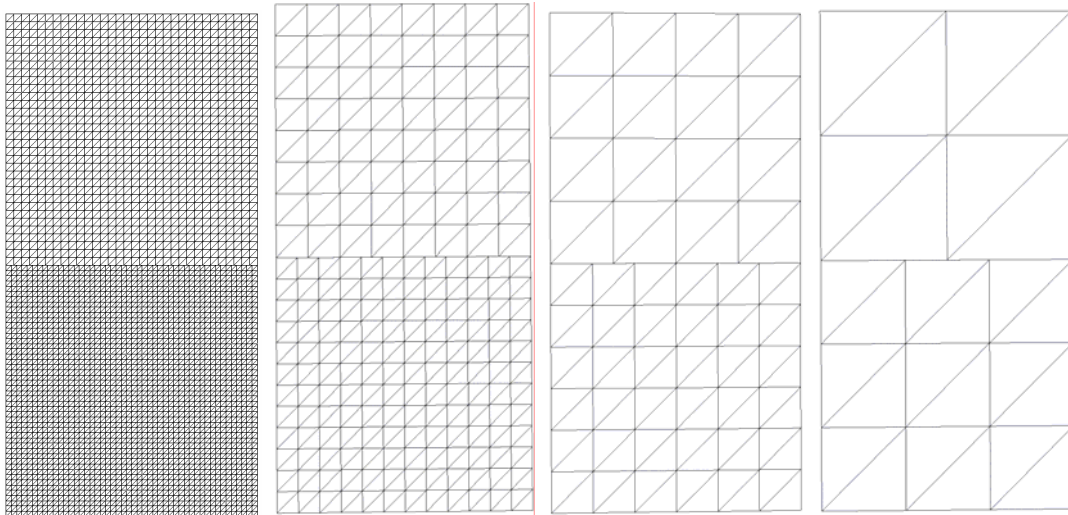


Figure 8: Non matching meshes for the convergence test: cases  $n^{\circ}1$ ,  $n^{\circ}2$ ,  $n^{\circ}3$ ,  $n^{\circ}4$

Figure 9 shows the obtained relative error versus the total number of degrees of freedom, with both Standard and Quasi-Symmetric contact formulations. With matching meshes, both formulations provide the same results, which are regarded as the reference ones. Globally, the obtained results are also quite similar to the ones with non matching meshes: it shows that both methods are quite satisfactory for this level of incompatibility of contact surfaces. This test is not very severe, but shows that the Quasi-Symmetric method behaves similarly to the Standard one and its results are always better.

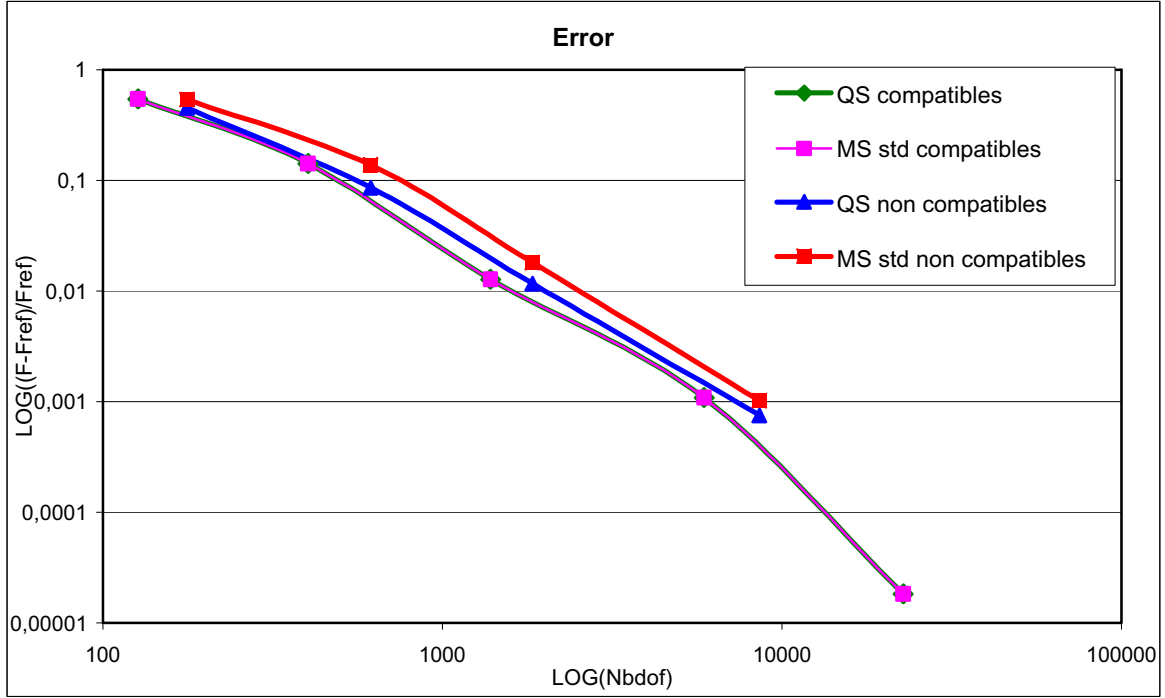


Figure 9: Convergence rates of the Standard and Quasi-Symmetrical formulations for the studied upsetting test: error versus number of degrees of freedom in logarithmic scale.

#### 4.2. Contact patch test

The studied contact patch test is described in [2]. Two cubes are piled up on a plane. The contact between them is bilateral and sticking. The lower cube is the slave body and has a uniform mesh, while the upper one is the slave body and has a refined mesh with same number of elements, as shown in Figure 10 and Figure 11. Either a constant stress field ( $\sigma_{zz} = 65 \text{ MPa}$ ) or a constant displacement ( $d_z = 1 \text{ mm}$ ) is imposed on the upper cube, in the vertical direction. With the first type of boundary condition, the cubes are elastic with different Young moduli,  $E_{master} = 3 \cdot 10^4 \text{ MPa}$  and  $E_{slave} = 1.3 \cdot 10^4 \text{ MPa}$ , but same Poisson coefficients  $\nu_{master} = \nu_{slave} = 0$ , so that the stress at the interface is constant. The problem exact solution, a constant stress field in the  $z$  direction and in particular on the contact interfaces, is easily obtained with matching meshes (see Figure 13). As the meshes of both bodies have only one element in the vertical direction, the constant stress value is properly imposed on the master side of the contact interface. The mean and maximum relative errors are then calculated only for the slave elements as:

$$E_r = \frac{\sum_{slave\_elts} |\sigma_{zz} - \sigma_{zz}^{ref}|}{\sum_{slave\_elts} |\sigma_{zz}^{ref}|} \quad \text{and} \quad E_r^{\max} = \frac{\text{Max}_{slave\_elts} |\sigma_{zz} - \sigma_{zz}^{ref}|}{\text{Max}_{slave\_elts} |\sigma_{zz}^{ref}|} \quad (46)$$

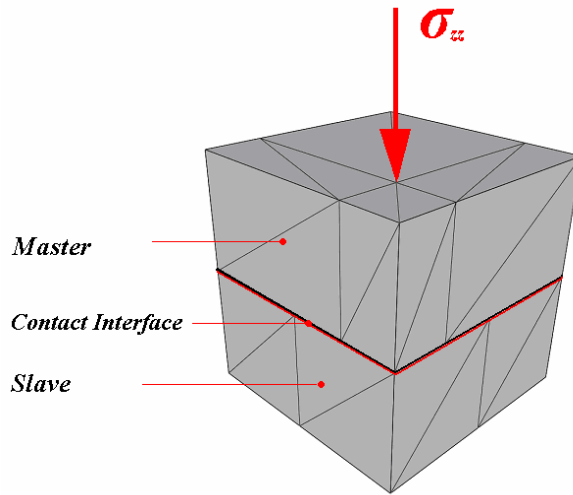


Figure 10: Contact patch test.

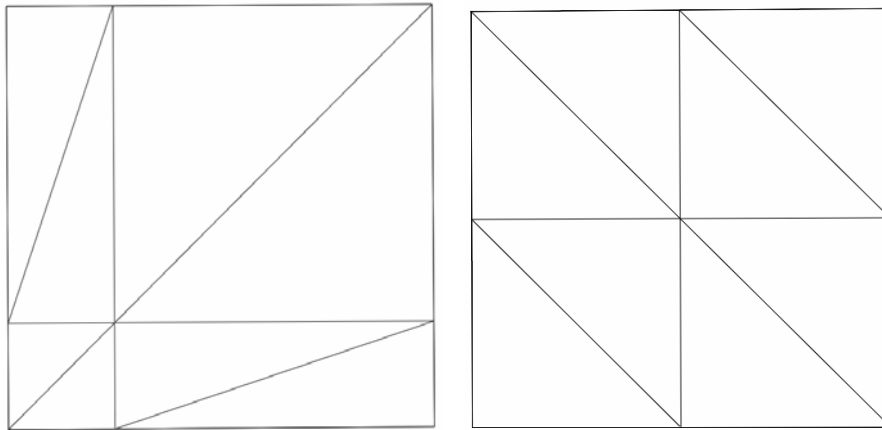


Figure 11: Contact patch test: master and slave contact interfaces.

In the second case, the cubes are Newtonians (viscoplastic with  $m=1$ ) with same consistencies,  $K_{master} = K_{slave} = 200 \text{ MPa}$ . The reference solution is calculated on a single cube, resulting from the merge of the two cubes.

Figure 12 summarizes the obtained results in the different cases for the mean error. They are quite similar to the obtained for the maximum error. They show that the Quasi-Symmetric formulation is always twice better than the Standard one. It also allows a much better transmission of the stress field through the interface, which can be qualitatively appreciated in Figure 14 and Figure 15, in comparison with the reference solution presented in Figure 13. However, it must be noticed that these figures have been obtained with a linear smoothing of the finite element stress field, which is actually constant by element. Although the finite element values are constant on the upper master body, because the Gauss points are not located at the same  $z$  coordinates, the nodal smoothing produces non uniform isovalues. On the contrary, the Gauss points of the lower slave body being vertically aligned, the visualized isovalues variations actually correspond to non uniform finite element values. Therefore, the analysis of these results must focus on the lower slave body and not take into account the artificial variations of the upper master one.

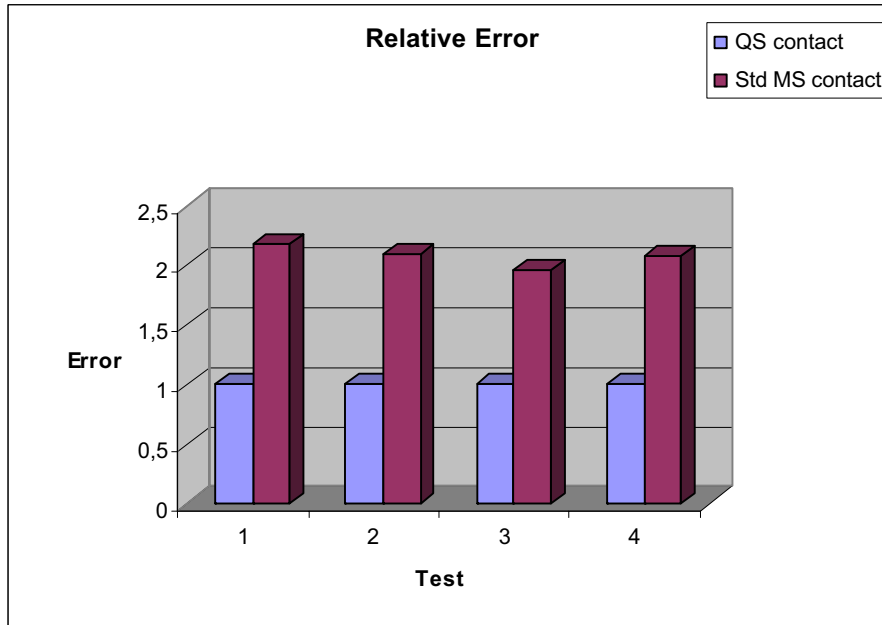


Figure 12: Relative error in the normal stress field transmission for the contact patch test using either the Standard or the Quasi-Symmetric formulation: in the elastic case, respectively for pressure (1) and velocity boundary conditions(2), and in the Newtonian case, respectively for pressure(3) and velocity boundary conditions(4).

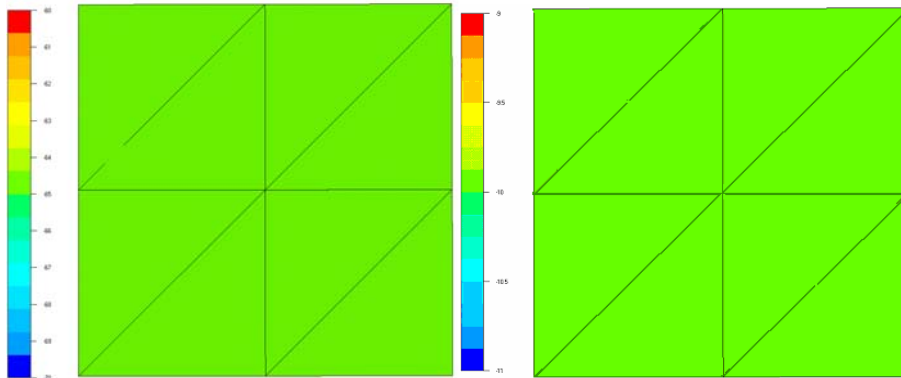


Figure 13: Contact patch test: perfectly constant stress field in the  $(0x,0z)$  plane for the reference solution with matching meshes, respectively with elastic and Newtonian materials.

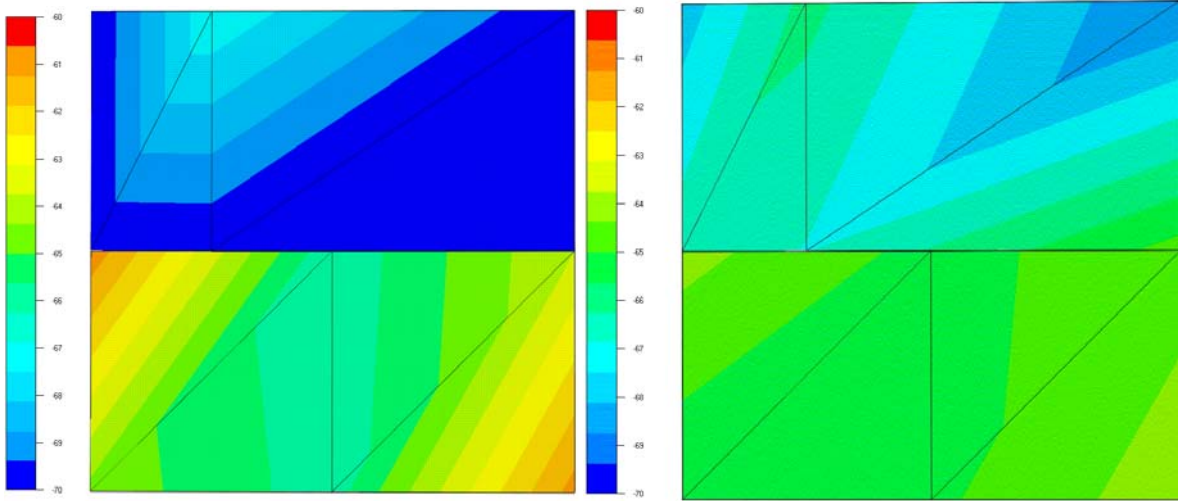


Figure 14: Contact patch test: stress field in the  $(0x, 0z)$  plane for the elastic materials, respectively with the Standard and Quasi-Symmetric formulations.

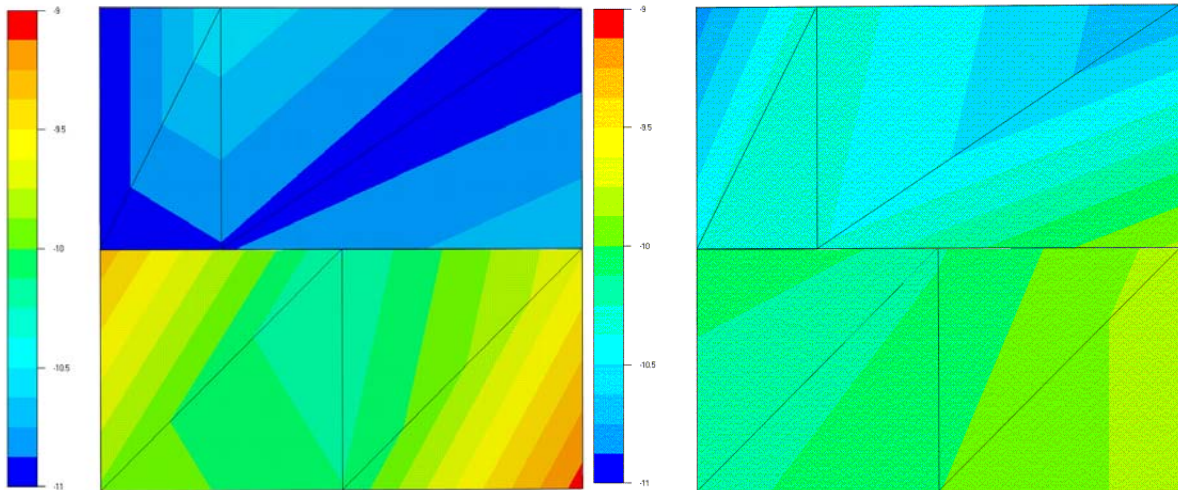


Figure 15: Contact patch test: stress field in the  $(0x, 0z)$  plane for the Newtonian material, respectively with the Standard and Quasi-Symmetric formulations.

As mentioned in [2], it should be noticed that this test is not a sufficient indicator to assess the contact algorithm quality. In fact, an over-constraint symmetrical formulation, like the two pass one, provides good results [2], because an artificially too stiff interface accurately transfer the stress field.

#### 4.3. Qualitative tests

In order to go further with the study of the stress field transmission, more qualitative studies have been carried out. The first one consists in upsetting two identical elastic cubes, with  $E = 3 \cdot 10^5$  MPa and  $\nu = 0.0$ , and which dimensions are: 20 mm x 20 mm x 10 mm. A constant stress field of 200 MPa is imposed on the upper cube (master) in the  $z$  vertical direction. As in the previous example, the stress field is constant at the interface and everywhere in the cubes, which is easily obtained with matching meshes. However, here, the master mesh is slightly finer than the slave one, as shown in Figure 16. This test is very similar to the convergence test of section 4.1, but rather than studying global values, such as the forging force, we more

precisely look to the contact interface. It results that the value of  $200 \text{ MPa}$  is not perfectly obtained, as can be seen in Figure 17 and Figure 18. The Standard formulation, although quite satisfactory when looking at global values (see section 4.1), exhibits significant discontinuities of the stress field near the contact interface (see Figure 17-left) and on the contact interface (see Figure 18-left) where a chessboard pattern is observed. These defects are quite significantly reduced with the Quasi-Symmetric formulation (see Figure 17-right), even on the interface itself (see Figure 18-right), so providing a much better and almost perfect solution, both locally and globally.

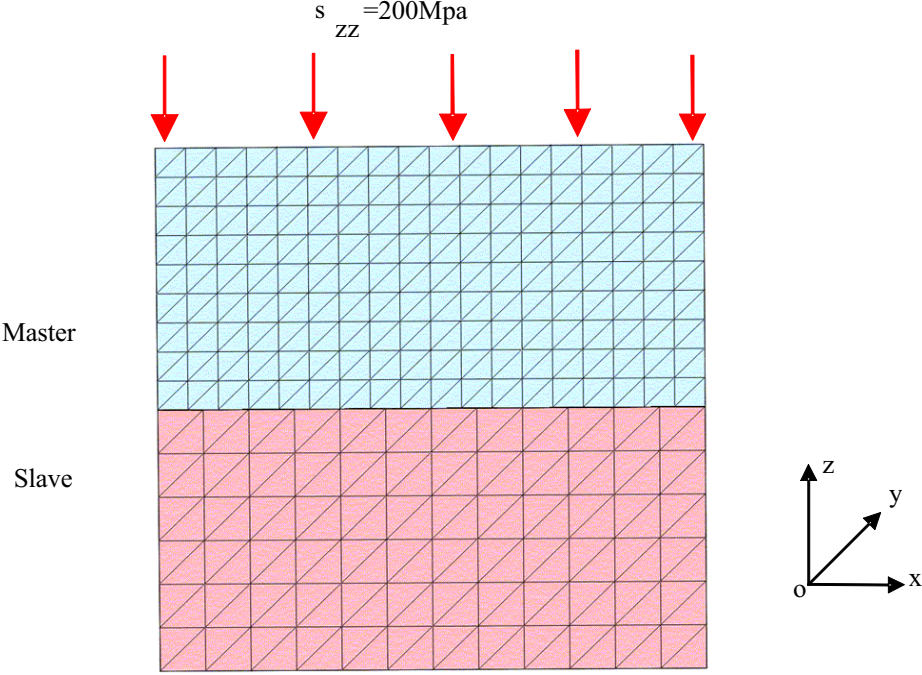


Figure 16: Constant normal pressure test: configuration and meshes.

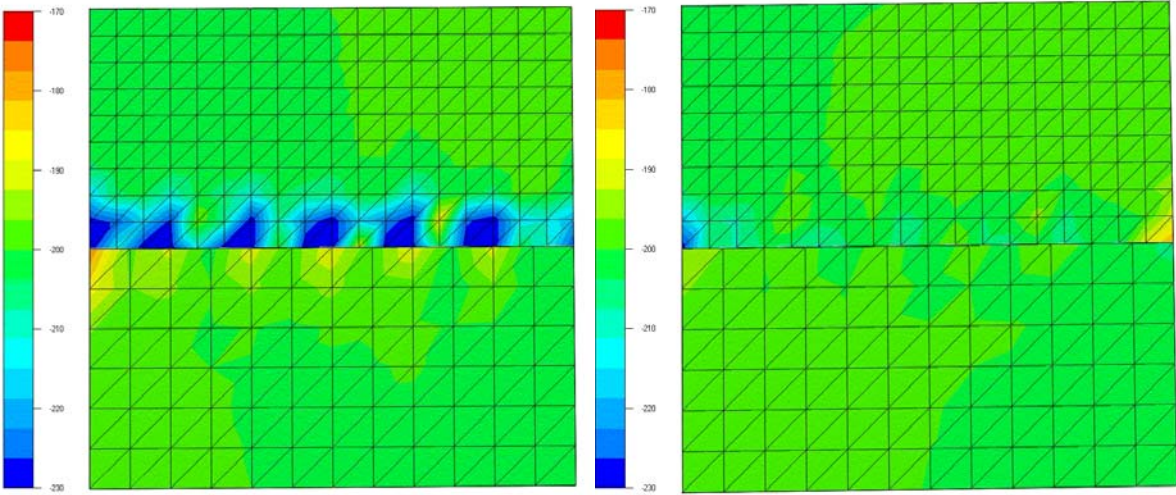


Figure 17: Constant normal pressure test:  $\sigma_{zz}$  isovalues in the  $(Ox, Oz)$  plane using the Standard and Quasi-Symmetric formulations

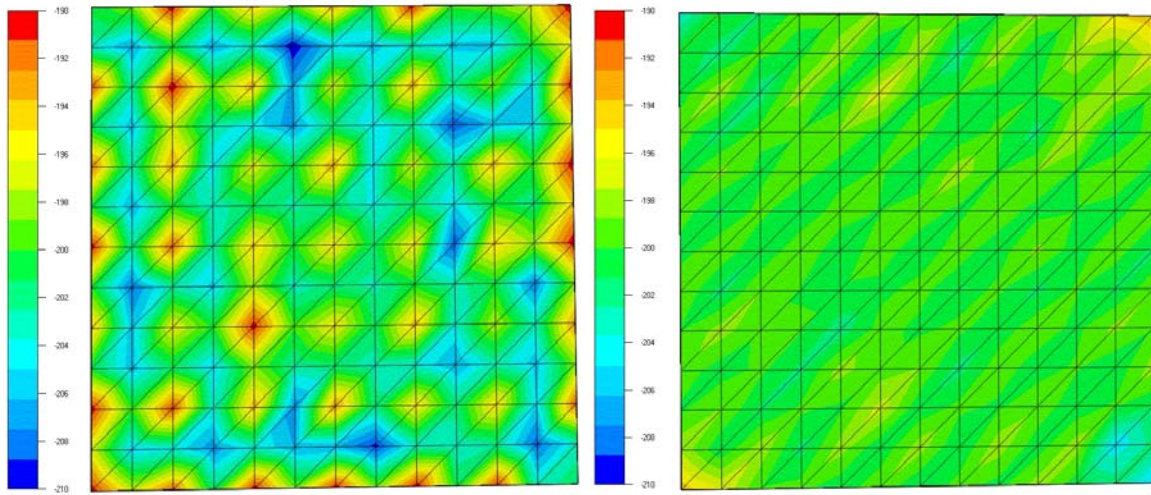


Figure 18: Constant normal pressure test:  $\sigma_{zz}$  isovalues in the  $(Ox,Oy)$  interface plane using the Standard and Quasi-Symmetric formulations

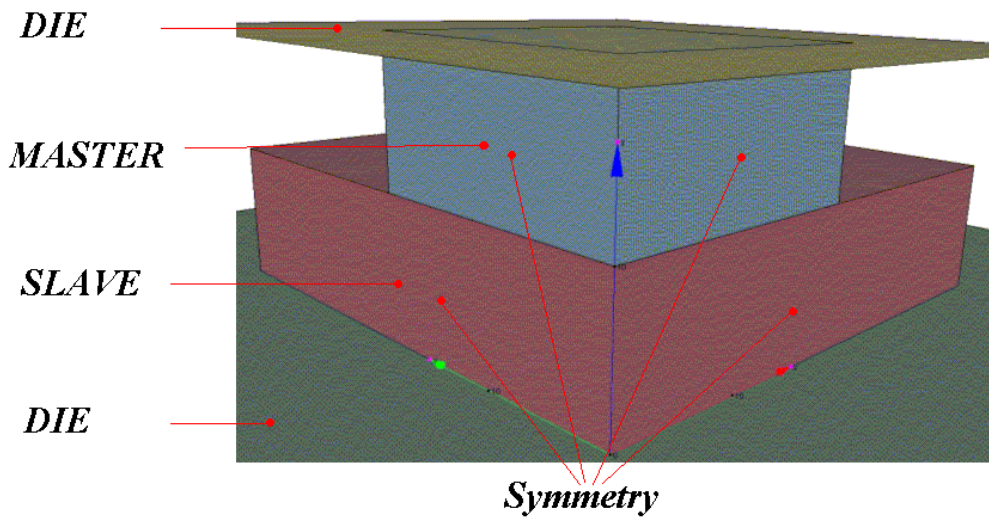


Figure 19: Configuration for the upsetting of a small cube into a larger one.

The next test consists into upsetting a small cube (40 mm x 40 mm x 10 mm) against a larger one ( 80 mm x 80 mm x 10 mm), as presented in Figure 19. Both cubes are made of Newtonian materials (viscoplastic with  $m=1$ ), the smaller being two times stiffer than the larger one:  $K_{small}= 200 \text{ MPa}$  and  $K_{large}=100 \text{ MPa}$ . The contact at their interface is perfectly sliding without friction. The reference solution in terms of forging effort is calculated with matching meshes, which size is  $h= 0.5 \text{ mm}$ :  $F_{ref}= 1.393 \text{ kgf}$ . Then, the smaller cube is discretized with a mesh size  $h= 1.0 \text{ mm}$ , and the larger one with  $h= 3.0 \text{ mm}$ . The relative error is calculated as in equation (45). The forging efforts are calculated alternatively with the smaller cube as master and as slave (the larger one being consequently slave and master) with both contact formulations. Results are summarized in Table 2.

<i>Mesh size</i>	<i>Fine Master</i>		<i>Fine Slave</i>	
	$h_{Master} = 1.0 \text{ mm}; h_{Slave} = 3.0 \text{ mm}$		$h_{Master} = 3.0 \text{ mm}; h_{Slave} = 1.0 \text{ mm}$	
<i>Formulation</i>	<i>QS</i>	<i>Standard</i>	<i>QS</i>	<i>Standard</i>
<i>Force</i>	1.42	1.09	1.44	1.44
<i>Error</i>	2.0 %	<b>22 %</b>	2.6 %	2.7 %

Table 2: Forging efforts and relative errors for the upsetting of the Newtonian cubes of different mesh sizes with different contact formulations and exchanging the functions of master and slave.

According to expectations, significant errors are obtained when the Standard formulation is used with a master body that has a much finer mesh. The error is 22%, about 8 times larger than when the functions of master and slave are exchanged (then only 2.7%). Figure 20 shows that the error comes from a high level of discontinuity of the velocity field on the contact interface, as several nodes of the master body are not loaded and wish to penetrate the slave body. With the Quasi-Symmetrical formulation, the results hardly depend on the choice of master and slave (errors of 2.0% and 2.6%). In the worst case, Figure 21 shows that there is still a high level of continuity of the velocity field on the interface, so providing a quite significant improvement with respect to Figure 20. On the other hand, it is noticed that when the master body is finer, the CPU time is notably increased.

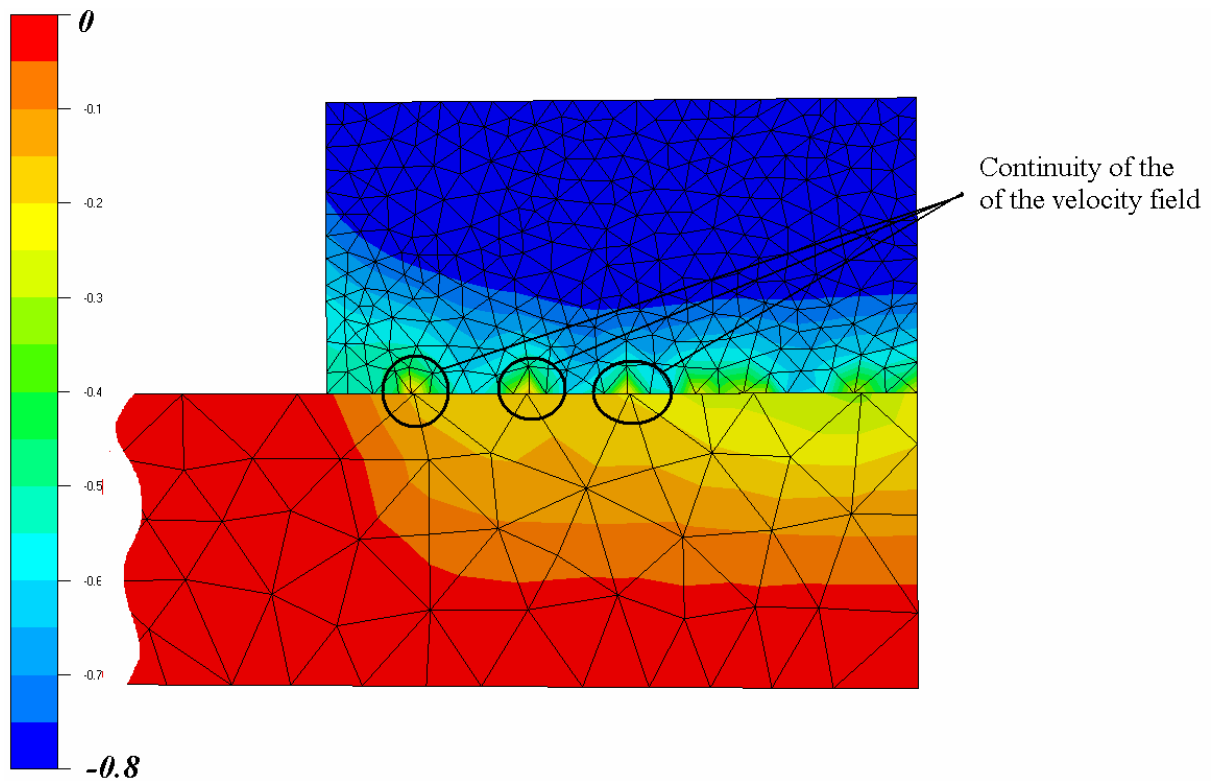


Figure 20: Isovalues of the velocity field in the vertical direction obtained with the Standard formulation, showing alternations of continuity and discontinuity on the contact interface.

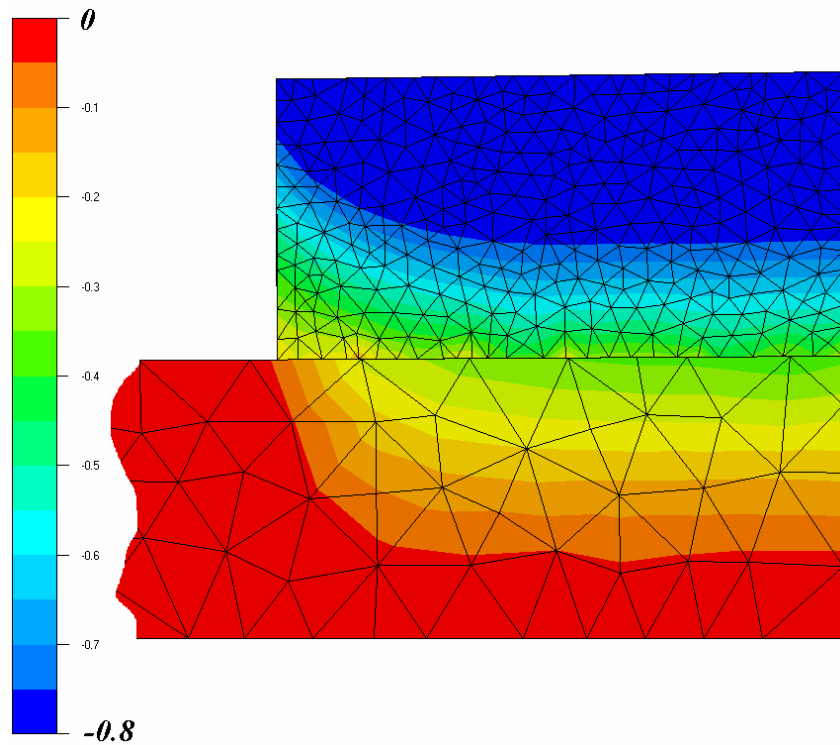


Figure 21: Isovalues of the velocity field in the vertical direction obtained with the Quasi-Symmetric formulation, showing high level of continuity on the contact interface.

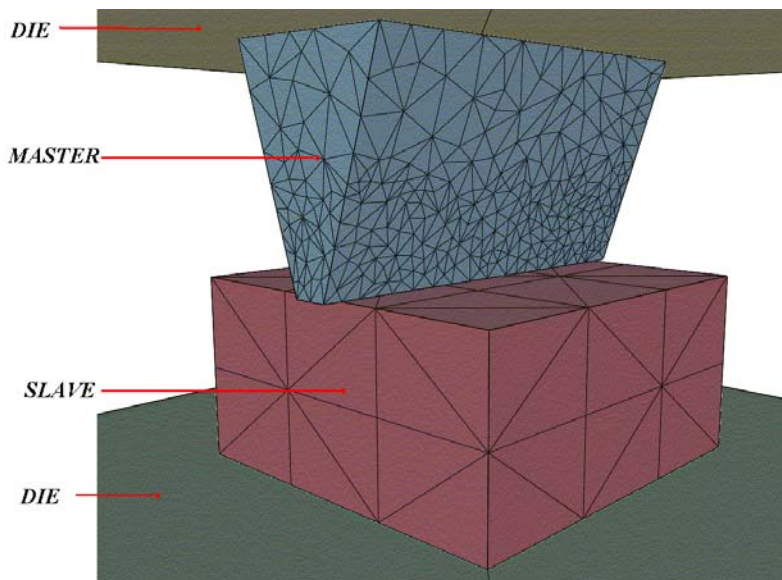


Figure 22: Indentation of a finely refined master body into a coarsely meshed slave body: configuration and meshes

The extreme case presented in Figure 3, for which the difference of mesh sizes between master and slave is very large, is recalled in Figure 22. The contact between the bodies is perfectly sliding, without friction. Both bodies are Newtonian, and the consistency of the

master body, the upper indenter, is 5 times larger the consistency of the slave one:  $K_{master}=100$  MPa and  $K_{slave}=20$  MPa. With this particular geometry and discretization, the Standard formulation fails completely, not being able to detect any contact phenomenon (see Figure 3-right and Figure 23-left). All nodes of the slave body are too far from the master obstacle to be regarded as belonging to the contact surface, which so is void. On the other hand, the Quasi-Symmetric formulation makes it possible to compute very large deformations (see Figure 23-right). It so provides proper loads on interface nodes, as shown by the high level of continuity of the velocity field in the vertical direction (Figure 24). In this case, all boundary conditions are coming from the contact analysis of the master surface, so only the additional term of equation (41) is active.

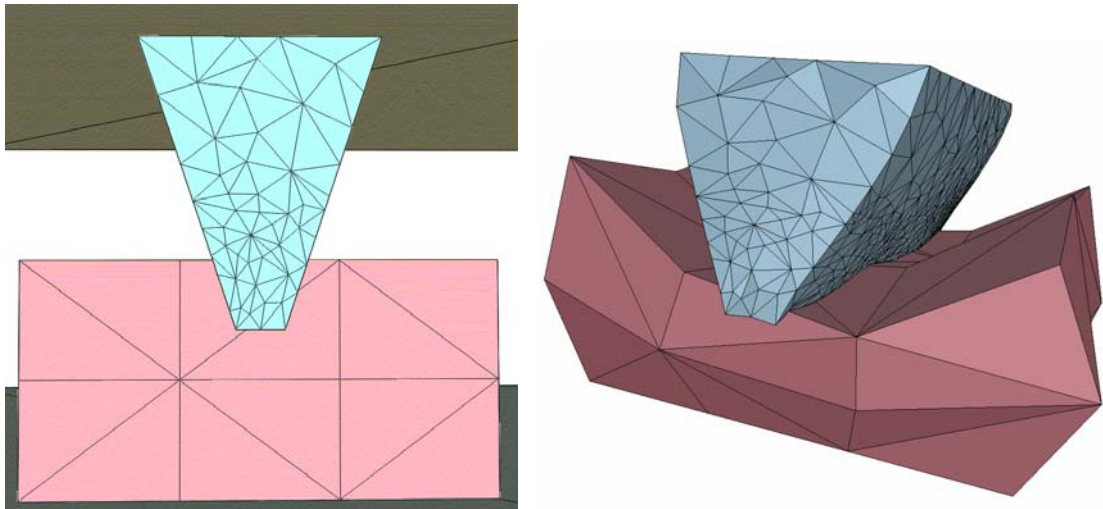


Figure 23: Simulation of the indentation process, respectively using the Standard and Quasi-Symmetric formulations

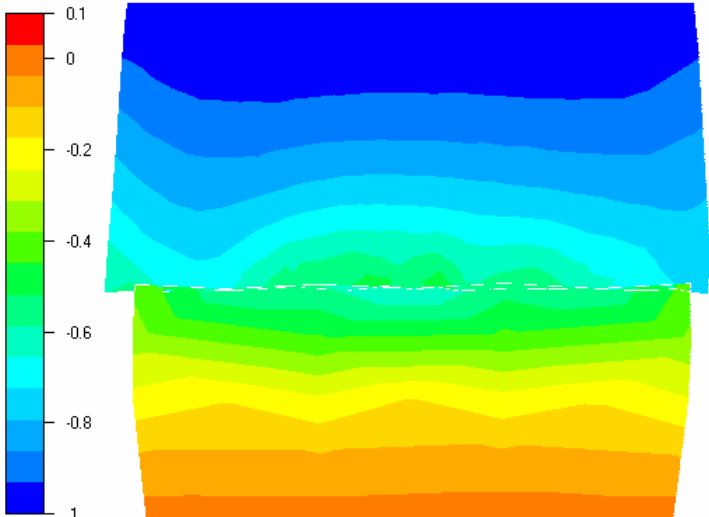
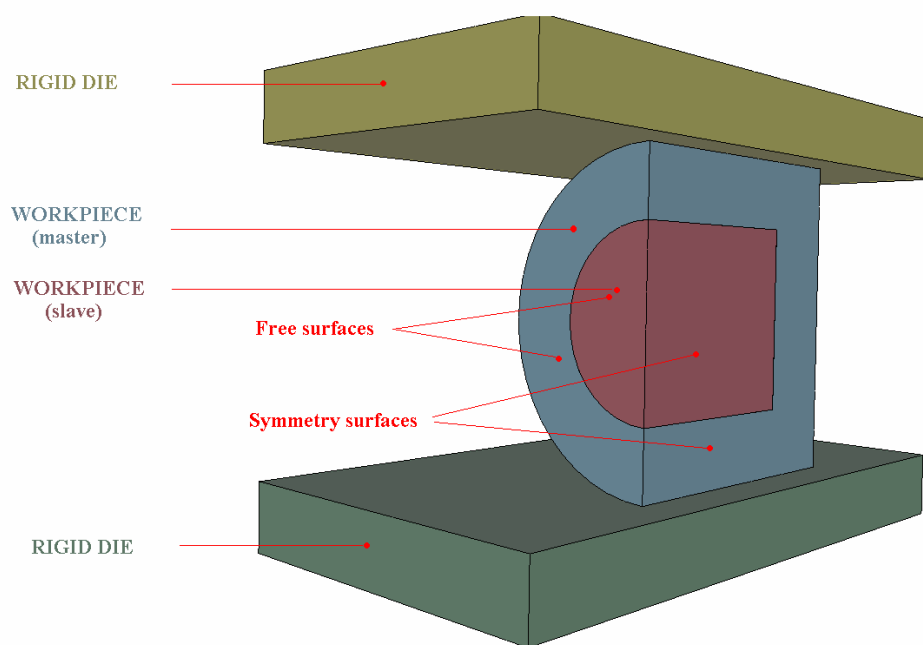


Figure 24: Cut in the middle of the parts showing the isovalues of the vertical velocity field obtained with the Quasi-Symmetric formulation.

## 5. APPLICATIONS



*Figure 25: Forging between flat dies of a component made of two embedded materials for the car industry.*

The Quasi-Symmetric formulation is then compared to the standard one for more complex applications that have been provided by the car industry. The first one, presented in Figure 25, consists in the upsetting of two embedded cylinders that are modeled by a rigid visco-plastic law with thermal softening. The exterior part, the master body, is stiffer than the interior one, the slave body, and the contact between them is regarded as perfectly sticking. The process simulation requires several remeshings of both bodies. Initially the slave mesh is finer, but latter on, the master mesh becomes finer (see Figure 26 and Figure 27). The integrated values, like the forging force and the numerical volume loss, that are obtained with both contact formulations are almost identical. The computational time is 93 minutes with the Standard formulation and 101 minutes with the Quasi-Symmetric one. The added value of this small increase of cost can be seen in Figure 28: the contact interface is much more accurately modeled without any detectable penetration of the master mesh into the slave one. This example shows the robustness of the Quasi-Symmetric formulation for taking into account the possible variations of relative mesh refinements, at a very low cost.

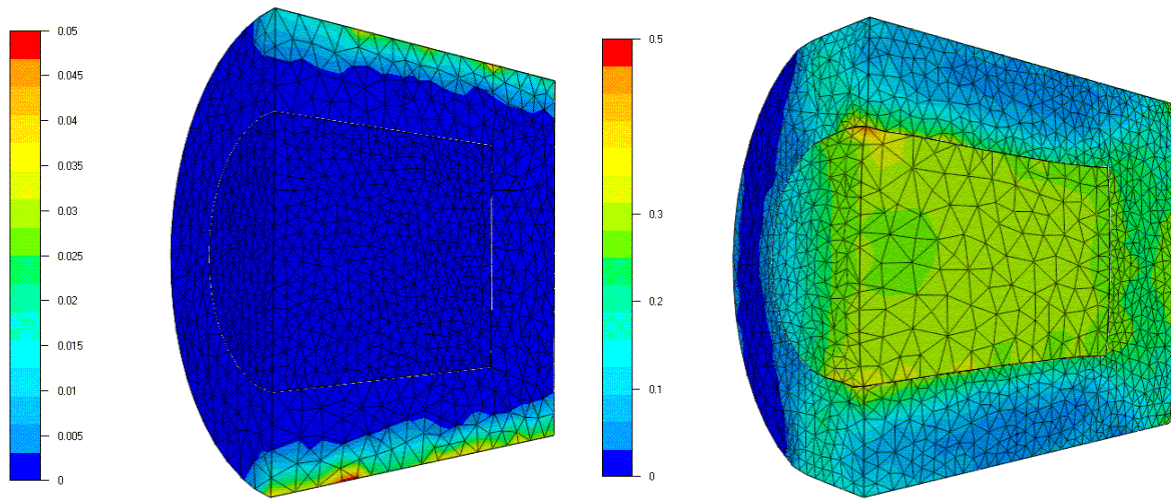


Figure 26: Isovalues of total deformation: beginning and middle of the process.

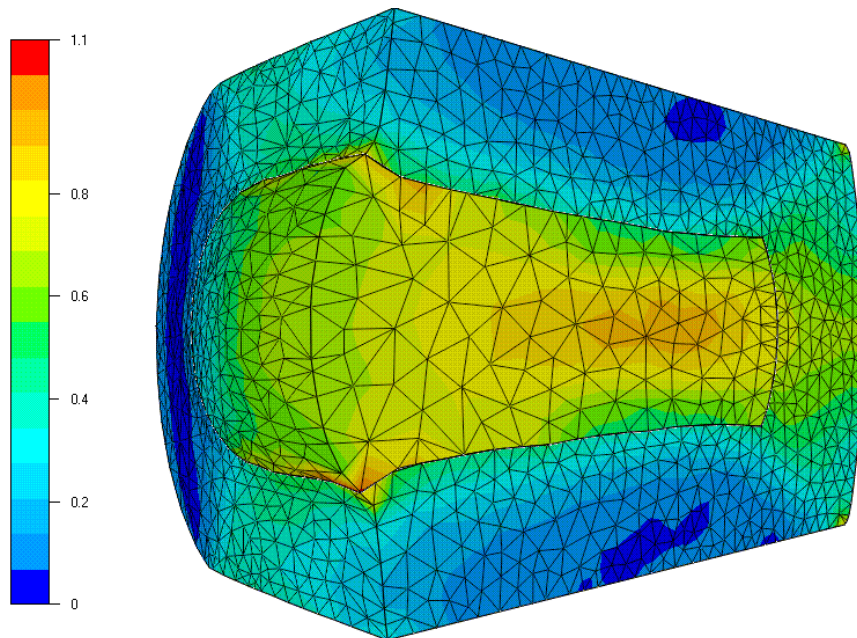


Figure 27: Isovalues of total deformation during forging: end of the process.

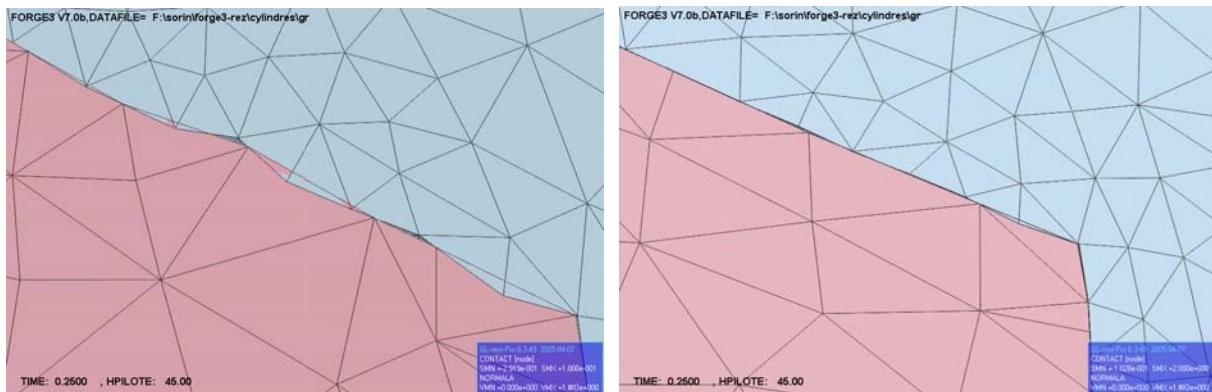


Figure 28: Zoom on the contact interfaces respectively obtained with the Standard and Quasi-Symmetric formulations.

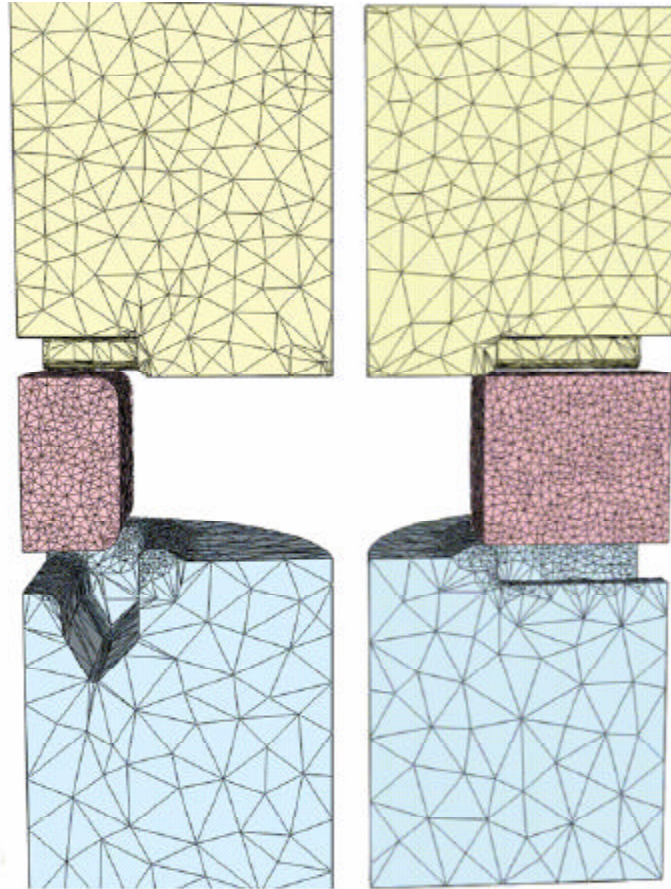
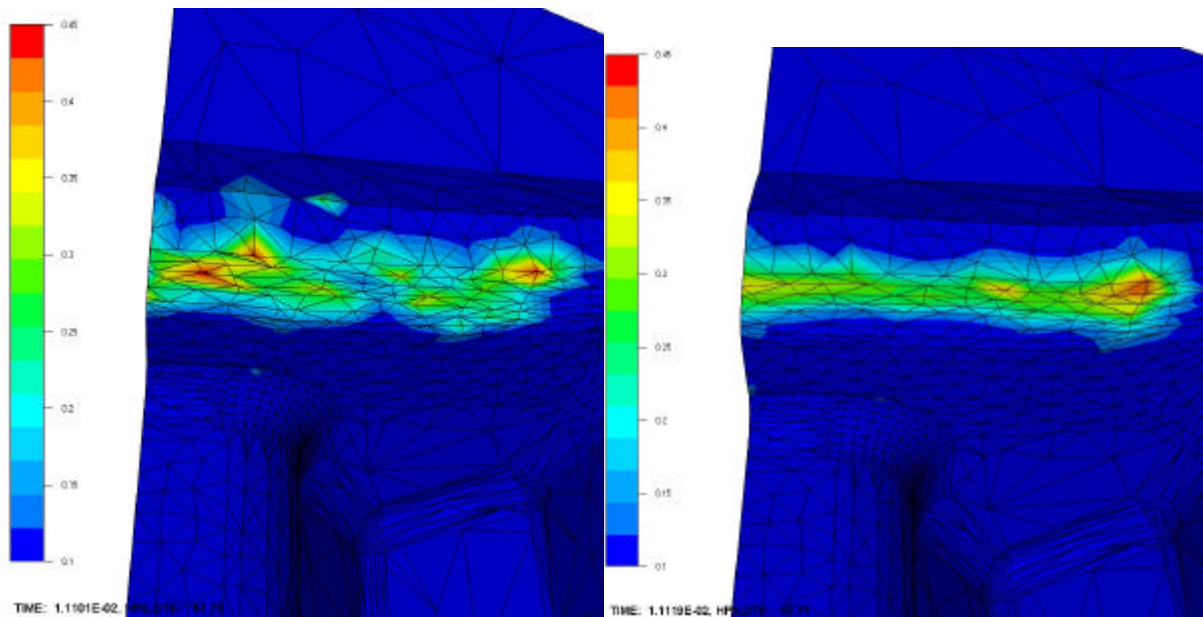


Figure 29: Simulation of the forging of a car component in order to study the die life: meshes of the workpiece and the part.



*Figure 30: Normal stress on the forging tools (master bodies) respectively with the Standard and Quasi-Symmetric formulations.*

In the second hot forging example, presented in Figure 29, the objective is to study the tool life due to the thermo-mechanical cycles during the mass production process. The workpiece is supposed to obey a rigid thermo-visco-plastic law while the tools are thermo-elastic. In this case, it is natural to select the workpiece as the slave body, because it undergoes the most severe deformations, and the upper and lower tools as master bodies. However, in order to accurately compute the thermo-mechanical stresses on the ribs of the tools, the dies are locally more finely meshed than the workpiece. As a matter of fact, when using the standard contact formulation, the stress distribution is not correct of the tool, as shown in the left part of Figure 30, where classical oscillations of the stress field are observed. Using the Quasi-Symmetric formulation allows computing a stress field that is quite satisfactory (see the right part of Figure 30).

## **6. CONCLUSIONS**

The proposed Quasi-Symmetric contact formulation is rather easy to implement into an existing finite element software. It can be equally utilized with an integral (facet-to-facet) or a nodal (node-to-facet) formulation, our numerical tests having been done with the latter in the FORGE3® software. It basically requires two analysis of the contact conditions, in a symmetric way, which so results in a small increase of the computational time with respect to the standard formulation. The additional cost is about 10% in the studied industrial applications. A noticeable increase of CPU time has been only observed in a very particular test case, with a very fine master body. It is due to the increase of the system local bandwidth and to the consequent deterioration of the matrix conditioning caused by these extra diagonal terms.

The numerical tests clearly demonstrate the superiority of the Quasi-Symmetric contact formulation over the Standard one. When the Standard formulation provides satisfactory results, the Quasi-Symmetric formulation exhibits a similar convergence rate with a better accuracy. Its results are almost identical to the ones obtained with other methods, like the Integral Joint formulation or the Mortar approach. Moreover, they are almost independent on the choice of the master and slave body, even when the discretisation of the two contacting bodies are very different, which so validates its Quasi-Symmetric attribute. It so allows solving all the encountered shortcomings of the standard formulation, with a reduced increase of computational time: accurate calculations on a finely meshed master body and detection of small obstacles with a coarse slave mesh.

## **ACKNOWLEDGEMENTS**

The authors gratefully acknowledge support from the French government and the companies involved in the SIMULFORGE project managed by CETIM.

## REFERENCES

- [1] J.-L. Chenot, L. Fourment, K. Mocellin, Numerical treatment of contact and friction in FE simulation of forming processes, *J. Mater. Process. Technol.* 125-126 (2002) 45-52.
- [2] N. El-Abbasi, K. J. Bathe, Stability and patch test performance of contact discretizations and a new solution algorithm, *Comput. Struct.* 79 (2001) 1473-1486.
- [3] M. A. Puso, T. A. Laursen, A mortar segment-to-segment frictional contact method for large deformations, *Comput. Methods Appl. Mech. Eng.* 193 n° 45-47, (2004) 4891-4913.
- [4] P. Hild, Numerical implementation of two nonconforming finite element methods for unilateral contact, *Comput. Methods Appl. Mech. Eng.* 184 n° 1, (2000) 99-123.
- [5] J. R. Fernandez, Numerical analysis of a contact problem between two elastic-viscoplastic bodies with hardening and nonmatching meshes, *Finite Elements Anal. Des.* 40 n° 7, (2004) 771-791.
- [6] N. El-Abbasi, K. J. Bathe. , On a New Segment-to-Segment Contact Algorithm, *Computational Fluid and Solid Mechanics*, K.J. Bathe. Eds. 2001
- [7] L. Baillet, T. Sassi, Mixed finite element formulation in large deformation frictional contact problem, in: E. O. a. D. R. J. Owen Eds.VII International Conference on Computational Plasticity CIMNE, 2003.
- [8] M. A. Puso, T. A. Laursen, A mortar segment-to-segment contact method for large deformation solid mechanics, *Comput. Methods Appl. Mech. Eng.* 193 n° 6-8, (2004) 601-629.
- [9] A. M. Habraken, S. Cescotto, Contact between deformable solids: the fully coupled approach, *Mathl.Comput.Modelling* 28 n° 4-8 (1998) 153-169.
- [10] J. R. Fernandez Garcia, P. Hild, J. M. Viano, Resolution numerique d'un probleme de contact entre corps elasto-viscoplastiques et maillages elements finis incompatibles, *Comptes Rendus de l'Academie des Sciences - Series I - Mathematics* 331 n° 10, (2000) 833-838.



## **CONCLUSIONS AND PROSPECTS**



## CONCLUSIONS AND PROSPECTS

### *Conclusions*

This study intends to increase the performances and accuracy of the Forge3® simulation software. The first part of this work provides a practical CPU time reduction strategy for a particular class of problems having repetitive configurations.

Firstly, the recurrent boundary conditions have been imposed only for the workpiece, both for the mechanical and thermal problems, using a Master/Slave algorithm derived from deformable bodies contact. The applications show that using this approach the recurrent boundary conditions can be properly imposed, even if the standard usual Master/Slave algorithm have limitations. When forging helical gears, it is not very likely to have very different refinements of the meshes of the two symmetry surfaces, so the drawbacks of the Master/Slave algorithm are not critical.

Then this algorithm have been extended to several bodies, using the “ghosts” tool strategy. It so allows to carry out simulations on only one tooth of the workpiece and one tooth of the deformable tool even if a Lagrangian formulation is used and the two parts can have different deformations.

The second part of the thesis offers a reliable solution to avoid the problems of the standard Master/Slave contact formulation, without obtaining a prohibitive CPU time. The quasi-symmetrical approach seems a very promising solution to handle deformable bodies contact in 3D. It provides good accuracy both of imposing a velocity field or a stress field, almost independent of the mesh sizes of the contact interfaces of the bodies in contact.

After implementing and testing the contact approach, the symmetrical friction was the natural strategy to complete the mechanical boundary conditions between deformable bodies.

### *Prospects*

Any improvement of the contact formulations can ameliorate the recurrent boundary conditions, so, putting together the two parts of this thesis, applying recurrent boundary conditions using a quasi-symmetrical algorithm becomes an obvious task for the future developments.

As for the quasi-symmetrical contact, the thermal problem is to be handled. Also, the symmetrical friction has only been evaluated qualitatively, so a rigorous test series should be designed and carried out to investigate it more precisely.

Also, all the developments done in parallel in our laboratory should be integrated. Especially, the adaptive remeshing developed by Mr. Ramzy Boussetta can use the quasi-symmetrical contact handling, knowing that an excessive refinement of the master body can be obtained in order to minimize the estimated error. In this case, at the next time step, the stress field of the master interface is not accurate and the error estimators can provide wrong results leading to a improper mesh adaptation of the next increment.



## **REFERENCES**



**REFERENCES**

- [ABBA 01] N. El-Abbasi and K-J. Bathe, *Stability and patch test performance of contact discretisations and a new solution algorithm*, Computers and Structures 79, 2001
- [AGAS 96] J. Agassant, P Avenas, J-Ph. Sergent, B. Vergers and M. Vincent, *La Mise en forme des matières plastiques*. Lavoisier TEC&DOC, 1996
- [ALIA 00] C. Aliaga, *These de doctorat*, Centre de Mise en Forme des Materiaux, 2000
- [AREI 03] Areias, P.M.A and César de Sa, J.M.A, *Contact Between Deformable Solids: A New Second Order Approach*, VII International Conference on Computational Plasticity COMPLAS VII, Barcelona 2003
- [BAILL 03] L. Baillet, T. Sassi, *Mixed finite element formulation in large deformation frictional contact problem*, VII International Conference on Computational Plasticity COMPLAS VII, Barcelona 2003
- [BARB 02] Barboza J., Fourment L and Chenot J-L, *Contact algorithm for 3D multi-bodies problems: application to forming of multi-material parts and tool deflection*. In WCCM V - Fifth Congress on Computational Mechanics. 2002. Wien, Austria
- [BARB 04] J. Barboza, *Traitement du contact entre les corps déformables et calcul parallèle pour la simulation 3D du forgeage multicorps*, Thèse de doctorat, Centre de Mise en Forme des Matériaux, Ecole des Mines de Paris, Sophia Antipolis 2004.
- [BATH 01] Bathe K.J. and Abbasi N.E., *On a new Segment to Segment Contact Algorithm*, in *Computational Fluid and Solid mechanics*, K.J Bathe, Editor. 2001, Elsevier Science
- [BELL 94] M. Bellet, *Mécanique et thermique des milieux continus*. Séminaire de plasticité Eléments finis et mise en forme des métaux, volume1, Centre de Mise en forme des Matériaux, Ecole des Mines de Paris, Sophia Antipolis Septembre 1994
- [CESC 01] S. Cescotto, *On the Numerical Modelling of Unilateral Contact: Primal, Dual and Mixed Approaches*, The 8<sup>th</sup> Conference of Enhancement of Computing Methods for Engineering and Science, Shanghai, 2001
- [CHAB 98] P. Chabrand, F. Dubois and M. Raous, *Various numerical methods for solving unilateral contact problems with frictions*. Mathematical and Computer Modelling, 1998
- [CHEN 98] J-L Chenot and L. Fourment, *Numerical formulations and algorithms for solving contact problems in metal forming simulation*. Computational Mechanics, E Onate and S.R Idelsohn (eds), Barcelona, Spain, 1998

## REFERENCES

- [CRIS 00] M.A. Crisfield, *Re-visiting the contact patch test*, International Journal for Numerical Methods in Engineering 48, 2000
- [FERN 03] J.R. Fernandez, P. Hild and J.M. Viano, *Numerical Approximation of the Elastic-Viscoplastic Contact Problem with No-matching Meshes*. Numerical Mathematics 94, 2003
- [FOUR 98] L. Fourment, J-L. Chenot, K. Mocelin, *Numerical Formulations And Algorithms For Solving Contact Problems In Metal Forming Simulation*. International Journal for Numerical Methods in Engineering, 1999
- [FOUR 04] Fourment L., Popa S. and Barboza J., *A Quasi-symmetric Contact Formulation For 3D Problems. Application To Prediction Of Tool Deformation In Forging* – The 8th Conference On Numerical Methods in Industrial Forming Processes, Columbus, Ohio, USA, June 2004
- [HABR 96] A.M. Habraken and S. Cescotto, *Contact Between Deformable Solids. The Fully Coupled Approach*, Special Issue of JI. of Mathematical and Computer Modelling, 1996.
- [HILD 98] *Problèmes de contact unilatéral et maillages éléments finis incompatibles*, Thèse de Doctorat, Université Paul Sabatier de Toulouse, 1998
- [PARK 97] Park Y.B. and Yang D.Y., *Finite element analysis for precision cold forging of helical gear using recurrent boundary conditions*, Proc Instn Mech Engrs Vol 2/2 Part B, 7 October 1997
- [PAVA 96] Ch. Pavanachand and R. Krishnalumar. *A new one-pass approach for large deformation multibody frictional contact analysis*. Numerical Methods in Engineering, 1996
- [PICH 01] Pichelin E., Mocelin K, Fourment L. and Chenot J-L, *An application of a master slave algorithm for solving 3D contact problems between deformable bodies in forming processes*, Revue Européenne des Eléments Finis, 10-8 [2001] 857-880
- [TAYL 91] R.L. Taylor and P. Papadopoulos, *On a patch test for contact problems in two dimensions*. In P. Wriggers, W. Wagner (eds). Computational methods in non-linear mechanics. Springer, Berlin 1991
- [TERZ 04] L. Terzolo, *Vers une prédiction de la durée de vie des outils de forge a chaud par la détermination numérique du régime thermique et usure abrasive*, Thèse de Doctorat, Centre de Mise en Forme des Matériaux, Ecole des Mines de Paris, Sophia Antipolis 2004
- [WRIG 99] P. Wriggers and A. Rieger. *Adaptive methods for contact problems, recent developments*. European Conference and Computational Mechanics, Munchen, 1999

## Résumé

La simulation numérique de la mise en forme est un outil indispensable pour réduire les coûts de conception dans l'industrie. Le logiciel d'analyse éléments finis FORGE3® fut créé dans ce but et il est capable de résoudre des problèmes thermomécaniques des grandes déformations complexes, en prenant en comptes des lois de comportement non-linéaires et plusieurs corps déformables.

Dans la première partie de cette thèse on présente les travaux effectués pour prendre en compte les symétries cycliques de répétition afin de réduire le temps CPU pour la simulation thermomécanique du forgeage des engrenages hélicoïdaux. Ce type de symétrie est traité comme une condition de contact bilatéral collant particulière entre deux faces de symétrie appartenant au même corps, à travers d'un algorithme maître-esclave. Ensuite une technique similaire est utilisée pour traiter le contact entre la pièce et les outils déformables tout en gardant un domaine réduit sur lequel on effectue les calculs. Une première série des tests montre la fiabilité de la méthode.

La deuxième partie se focalise sur l'amélioration du traitement du contact entre les corps déformables, dont les maillages sont non coïncidents. On utilise une formulation nodale, quasi-symétrique pénalisée de la condition de contact. Cette approche nous permet d'appliquer des conditions aux limites sur tous les nœuds des interfaces sans surcontraindre le problème. Une deuxième série d'exemples académiques et industriels montre les avantages en terme de précision et de vitesse de convergence de la nouvelle méthode, d'une part, et la robustesse du code pour résoudre des problèmes industriels d'autre part.

**Mots clés :** mise en forme des matériaux, maître-esclave, symétries cycliques de répétition, outils déformables, contact quasi symétrique.

\*\*\*

## Abstract

In industry, the numerical simulation of material forming processes is a powerful method of cutting development costs. The finite element analysis software FORGE3® was created to solve large deformations thermo mechanical problems with non-linear material behavior and several deformable bodies.

The first part of this thesis presents the application of the repetitive symmetries necessary to reduce the CPU time for the helical gear forging simulation. This type of boundary condition is handled as a special bilateral sticking contact condition between the two symmetry surfaces of the same body, using a master-slave algorithm. Then a similar method is used to apply the contact conditions between the workpiece and the deformable tools, also running the simulation on a reduced domain. A first test series proves the reliability of this method.

The second part deals with the improvement of the deformable bodies contact condition with non-coincident meshes. A nodal penalized quasi-symmetric formulation is used to apply the contact equation. This approach allows applying proper boundary conditions on all the nodes of the two surfaces in contact without providing an over constraint problem. A second test series, both academic and industrial shows on one hand the improved accuracy and convergence rate of the new method, and on the other hand the reliability of the software when solving industrial problems.

**Keywords:** material forming, master-slave, recurrent symmetries, deformable tools, quasi-symmetric contact.